

Calibrating the metallicity of M dwarfs in wide physical binaries with F-, G-, and K-primaries - II: Carbon, oxygen, and odd-Z iron-peak abundances of the primary stars

C. Duque-Arribas,^{1*} H. M. Tabernero,¹ D. Montes¹ and J. A. Caballero²

¹ *Departamento de Física de la Tierra y Astrofísica & IPARCOS-UCM (Instituto de Física de Partículas y del Cosmos de la UCM), Facultad de Ciencias Físicas, Universidad Complutense de Madrid, 28040 Madrid, Spain*

² *Centro de Astrobiología (CSIC-INTA), camino bajo del Castillo s/n, 28691 Villanueva de la Cañada, Madrid, Spain*

Accepted 2024 January 4. Received 2023 December 07; in original form 2023 June 05

ABSTRACT

Detailed chemical composition of stars is of prime interest for a range of topics in modern stellar astrophysics, such as the chemical evolution of the Galaxy or the formation, composition, and structure of exoplanets. In this work, we derive the C and O abundances and update Sc, V, Mn, and Co abundances considering hyperfine structure effects (HFS) and correcting for non-local thermodynamical equilibrium (NLTE) for a sample of 196 late-F, G-, and early-K stars with wide resolved M-dwarf companions. We accomplished this by employing the equivalent width (*EW*) method and high-resolution spectroscopic data. Furthermore, we investigated the distributions of [X/Fe] ratios and [C/O] as a function of metallicity ([Fe/H]) and kinematic population. The observed trends are consistent with previous findings reported in the literature. Additionally, we searched for confirmed exoplanets around our primary stars in the literature and found 24 exoplanets in 17 systems, while none of the M-dwarf companions in our sample presented confirmed exoplanets. In conclusion, our study provides homogeneous abundances from high-resolution spectra for a large sample of FGK primary stars, paving the way for further research on stellar abundances of the M secondaries and exoplanetary science.

Key words: stars: abundances – binaries: visual – stars: fundamental parameters – stars: late-type – stars: solar-type

1 INTRODUCTION

Cool, low-mass M-type dwarf stars stand as widely interesting objects in astrophysics. Being the most abundant main-sequence stars in the Milky Way (Henry et al. 2006; Winters et al. 2015; Reylé et al. 2021), and having main-sequence lifetimes far longer than the present age of the Universe (Adams & Laughlin 1997), M dwarfs rank as excellent objects to study the structure and chemical evolution of the Galaxy (Bahcall & Soneira 1980; Reid et al. 1997; Chabrier 2003; Ferguson et al. 2017). Additionally, M dwarfs constitute relevant targets in the search for exoplanets, since their faintness and lower masses facilitate the detection of low-mass exoplanets in their habitable zone (Tarter et al. 2007; Kopparapu et al. 2014; Shields et al. 2016). As a result, new spectrographs have been developed specifically optimized for conducting exoplanet searches around M dwarfs, such as CARMENES (Quirrenbach et al. 2020; Ribas et al. 2023).

These studies could be increased with prior knowledge of stellar metallicity and abundances. However, this duty is often really challenging in the case of M dwarfs, whose spectra are complex and notoriously difficult to model due to the presence of prominent molecular features, in comparison to those of solar-type stars (e.g. Allard et al. 2000; Passegger et al. 2018; Marfil et al. 2021). For this reason, several studies have tried photometric calibrations of metallicity for M dwarfs (see Duque-Arribas et al. 2023, and references

therein). Other studies have investigated M-dwarf metallicities using wide physical binary systems formed by a F-, G-, or K-primary star and a M-dwarf companion (e.g. Woolf & Wallerstein 2006; Bean et al. 2006; Rojas-Ayala et al. 2010; Terrien et al. 2012; Mann et al. 2013, 2014; Newton et al. 2014; Montes et al. 2018; Ishikawa et al. 2020; Souto et al. 2020, 2022). These binary systems provide an excellent opportunity to test not only the metallicities of the M dwarfs with those for their warmer primaries, but also the chemical abundances for individual atomic species. This is the second item of a series of papers eventually aimed at calibrating the metallicity of M dwarfs in wide physical binary systems with solar-type stars. However, here we still focus mostly on the primary stars, especially on the carbon, oxygen, and odd-Z iron-peak abundances. As a result, a calibration of the metallicity of the M dwarfs is not presented here yet, but we will do so in the next item of the series.

Oxygen and carbon are, after H and He, the most abundant chemical elements in the Universe. Carbon plays a role in dust formation processes in the interstellar medium (Leger & Puget 1984; Weingartner & Draine 2001; Draine & Li 2007), contributes significantly to the stellar interior and atmospheric opacity (Burrows et al. 1997; Baraffe et al. 1998; Meynet & Maeder 2002), and it is an essential element for life as we know it, being important in searching for biomarkers in habitable exoplanets (Des Marais et al. 2002; Scalo et al. 2007; Seager & Deming 2010). Furthermore, the oxygen abundance is used to map the chemical enrichment and star formation history of stellar populations in the Milky Way and to infer the metallicities from

* E-mail: chrduque@ucm.es

the H II regions (Tolstoy et al. 2009; Moustakas et al. 2010). The studies of C and O abundances have become more and more popular in recent years in the context of determining the composition of terrestrial exoplanets. Theoretical models predict that carbon-to-oxygen and magnesium-to-silicon ratios (C/O and Mg/Si) may provide information about the structure and composition of planets; the C/O ratio controls the distribution of Si among carbide and oxide species, while Mg/Si determines the silicate mineralogy (Larimer 1975; Bond et al. 2010; Suárez-Andrés et al. 2018). Recent studies suggest that elemental abundance ratios may differ when studied in host stars and in planetary atmospheres: some ratios such as Mg/Si and Fe/Si show similar values, but larger differences are found for C/O due to the dependence of the distance for volatile elements (Carter-Bond et al. 2012; Marboeuf et al. 2014; Thiabaud et al. 2015).

On the other hand, iron-peak elements, i.e. elements in the periodic table from Sc to Ge, are synthesised in thermonuclear explosions of supernovae and in Si-burning during explosive burning of core-collapse supernovae (Kobayashi 2016). However, the stellar yields of these elements are under debate (Kobayashi et al. 2020). In particular, the accurate determination of the abundances for odd-Z iron peak elements (Sc, V, Mn, and Co) require non-local thermodynamic equilibrium modelling of spectral lines taking into account the hyperfine structure splitting. These elements are relevant in several astrophysical analysis. For instance, manganese is fundamental in stellar population and nucleosynthesis studies to constrain the physics of SNe Ia (Seitenzahl et al. 2013). Cobalt is an interesting element in regard to the galactic chemical evolution, but there are disagreements about the overall abundance trend of Co in the halo and disc and about its nucleosynthesis production (Bergemann et al. 2010). Additionally, scandium holds significance in comprehending Am and Fm stars, which exhibit an overabundance of iron-peak elements but a deficiency in scandium and calcium.

In the first paper of this series (Montes et al. 2018, hereafter referred to as Paper I), we established a sample of 192 wide physically-bound systems, derived precise stellar atmospheric parameters (T_{eff} , $\log g$, ξ , and chemical abundances for 13 atomic species) for the primary stars using the equivalent width (EW) method and high-resolution spectra, under the local thermodynamic equilibrium (LTE) assumption, and performed a kinematic analysis, classifying the stars in different Galactic populations and stellar kinematic groups. In this second paper, we update the abundances of scandium (Sc), vanadium (V), manganese (Mn) and cobalt (Co) taking into account hyperfine structure (HFS) and non-local thermodynamic equilibrium (NLTE) effects, and determine new abundances for carbon (C) and oxygen (O). The LTE approximation simplifies energy distribution through particle collisions, but it becomes less accurate close to the stellar surface, where the radiation field deviates from being local, isotropic, and Planckian (Steenbock & Holweger 1984; Rutten 1988; Thévenin & Idiart 1999). Additionally, interactions between electron and nuclear spins of species with non-zero nuclear spin cause energy states to split, resulting in multiple components in the absorption line of the corresponding transition (Abt 1952; Kurucz 1993; Jofré et al. 2017; Heiter et al. 2021).

This paper is organised as follow. In Sect. 2 we describe the sample, line list and abundance analysis, indicating our solar abundances compared with previous results. Sect. 3 reports and discusses the results for C, O, Sc, V, Mn, and Co. Finally, Sect. 4 outlines our findings and presents an outlook for the future items of this series.

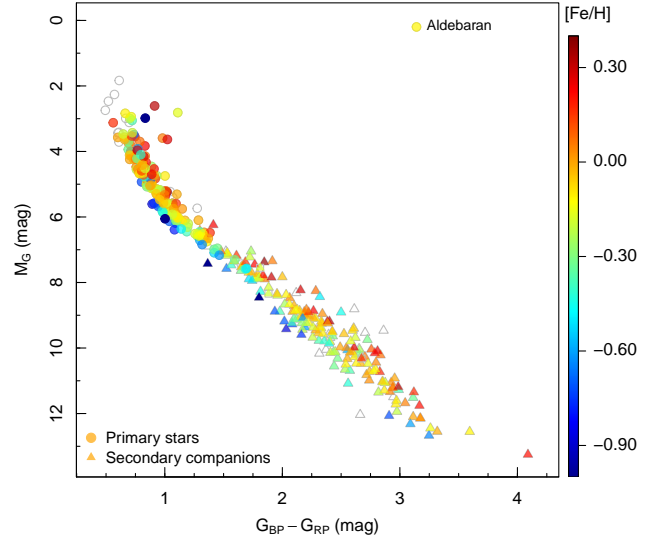


Figure 1. Colour-magnitude diagram of the primary and secondary stars in our sample using *Gaia* DR3 data, colour-coded by primaries’ $[Fe/H]$. Open data symbols are stars in systems whose primary is without derived stellar parameters.

2 ANALYSIS

2.1 Stellar sample

The sample used in this work was presented in Paper I and consists of 192 binary systems made of late-F, G-, or early-K primaries and late-K or M dwarf companion candidates. We carried out observations with the HERMES spectrograph (Raskin et al. 2011) at the 1.2 m Mercator Telescope at the Observatorio del Roque de los Muchachos (La Palma, Spain) and obtained high-resolution spectra for 196 FGK-type stars. These spectra were analyzed with the automatic code STEPAR¹ (Tabernero et al. 2019), which relies on the equivalent width method, to derive precise stellar atmospheric parameters (effective temperature T_{eff} , surface gravity $\log g$, microturbulence velocity ξ and iron abundance $[Fe/H]$) for 179 stars. However, we were not able to determine the stellar parameters of the rest stars due to factors such as double-line spectroscopic binaries, fast-rotating stars, too hot stars ($T_{\text{eff}} > 6700$ K) for not having enough iron lines, and too cool stars ($T_{\text{eff}} < 4500$ K) with too many overlapping iron lines. We re-analysed the proper motions and parallaxes of these systems using *Gaia* DR3 (Gaia Collaboration et al. 2022), confirming the results of Paper I. Therefore, we derived reliable spectroscopic stellar parameters for 174 primaries and 5 companions. For additional details on the basic properties of the studied systems and stellar parameters, please see Appendix B in Paper I. In Fig. 1 we show a colour-magnitude diagram of the primary and secondary stars in our sample.

2.2 Abundances, HFS effects, and NLTE corrections

To derive the carbon and oxygen abundances, we use the same line list as Tabernero et al. (2021), that is, C I lines at 5052.17, 5380.34, and 6587.61 Å and the O I infrared triplet lines at 7771.9, 7774.2 and 7775.4 Å. These C I lines can be perfectly described in LTE.

¹ <https://github.com/hmtabernero/StePar>

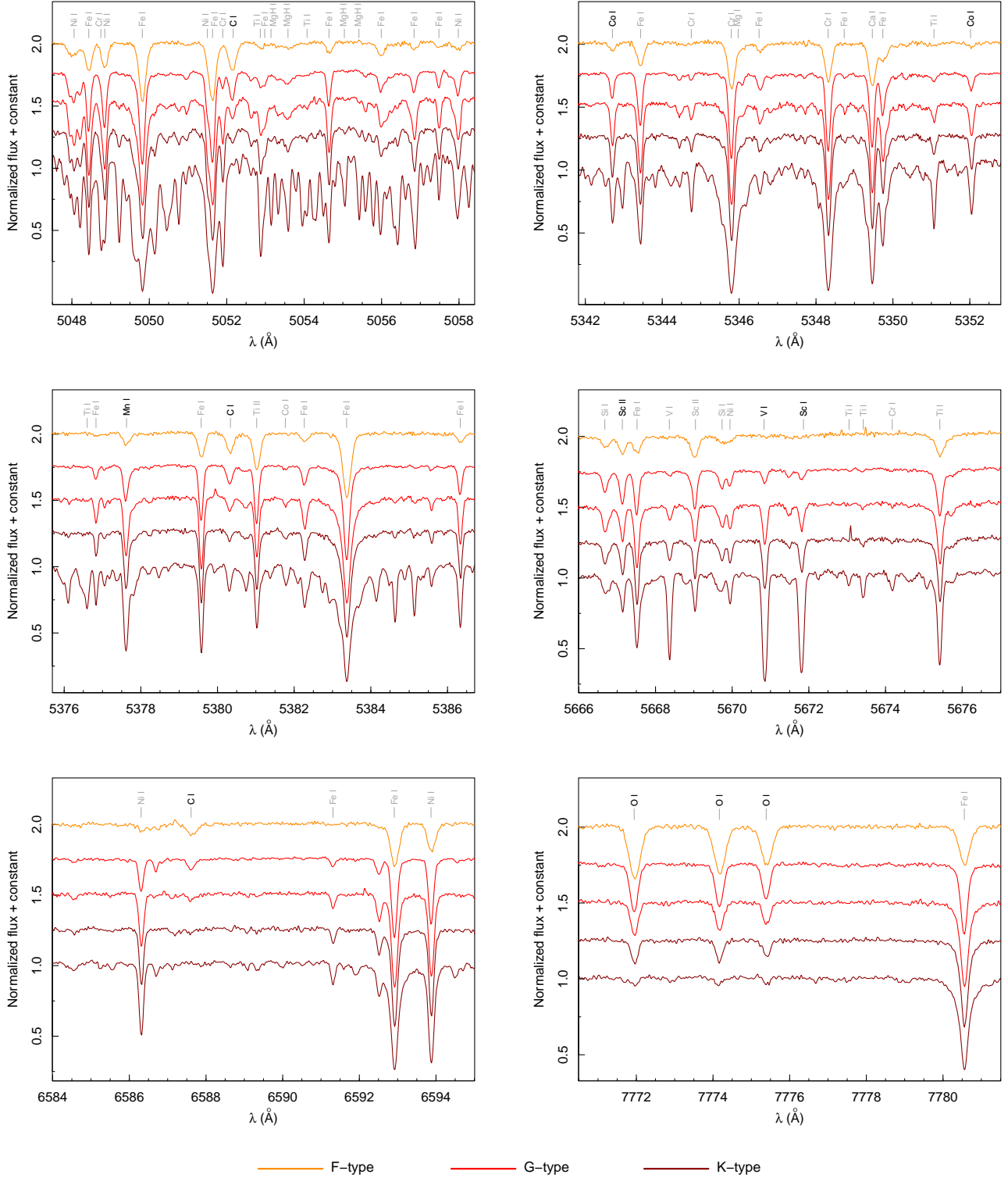


Figure 2. High-resolution spectra of five representative primaries from our sample of solar metallicity and different spectral types (*from top to bottom*): HD 35638 (F5 V), HD 43587 (G0 V), HD 82939 (G5 V), BD+68 1345 A (K0 V), and HD 6660 A (K4 V). Each panel shows zoomed ranges near some of the lines investigated.

Table 1. Atomic parameters for the lines used with the corresponding solar abundances in LTE, NLTE corrections, and number of HFS components.

Element	λ (Å)	$\log(gf)$	χ_I (eV)	$A(X)_{\odot}^{\text{LTE}}$	NLTE corr.	# HFS comp.
C I	5052.17	-1.304	7.68	8.359
C I	5380.34	-1.615	7.68	8.429
C I	6587.61	-1.021	8.54	8.327
O I	7771.944	0.369	9.15	8.779	-0.081	...
O I	7774.166	0.223	9.15	8.789	-0.070	...
O I	7775.388	0.002	9.15	8.769	-0.052	...
Sc I	5520.519	0.290	1.865	3.321	...	4
Sc I	5671.860	0.500	1.4478	3.037	...	21
Sc II	5526.789	-0.010	1.7682	3.207	...	20
Sc II	5657.886	-0.540	1.5070	3.265	...	13
Sc II	5667.135	-1.210	1.5004	3.248	...	7
Sc II	5684.190	-1.030	1.5070	3.116	...	9
Sc II	6245.621	-1.022	1.5070	3.011	...	15
Sc II	6320.832	-1.816	1.5004	3.059	...	7
V I	5670.831	-0.430	1.0806	4.002	...	21
V I	5737.027	-0.740	1.0636	3.906	...	16
V I	6081.461	-0.610	1.0509	3.901	...	10
V I	6224.520	-2.010	0.2866	4.074	...	21
V I	6251.802	-1.370	0.2866	3.895	...	21
V I	6274.659	-1.700	0.2670	4.005	...	6
V I	6285.162	-1.540	0.2753	3.971	...	12
Mn I	4502.204	-0.345	2.9197	5.347	+0.026	15
Mn I	4671.647	-1.675	2.8884	5.508	+0.030	15
Mn I	4739.072	-0.607	2.9408	5.402	+0.032	10
Mn I	5377.626	-0.166	3.8437	5.344	+0.042	12
Mn I	5399.500	-0.345	3.8530	5.481	+0.039	10
Mn I	5413.697	-0.647	3.8590	5.480	+0.036	6
Co I	4594.669	-0.042	3.6320	4.604	...	21
Co I	4792.854	0.001	3.2524	4.800	+0.111	18
Co I	4813.471	0.120	3.2158	4.849	+0.116	21
Co I	5301.017	-2.000	1.7104	4.953	+0.099	16
Co I	5342.706	0.741	4.0208	4.769	...	21
Co I	5352.020	0.060	3.5764	4.790	...	20
Co I	5359.188	0.244	4.1494	4.736	...	21
Co I	5647.207	-1.560	2.2800	4.883	+0.102	12
Co I	6814.958	-1.900	1.9557	4.774	+0.087	10

Stellar parameters for the Sun are $T_{\text{eff}} = 5777 \pm 18$ K, $\log g = 4.41 \pm 0.05$, and $[\text{Fe}/\text{H}] = 0.0$ dex ($A(\text{Fe}) = 7.48 \pm 0.01$ dex).

References for the NLTE corrections: O – Bergemann et al. (2021); Mn – Bergemann et al. (2019); Co – Bergemann et al. (2010) and Voronov et al. (2022).

On the other hand, the O I triplet, typically strong in solar-type stars and located in a spectral region free from other blending lines, is significantly affected by NLTE (Kiselman 1993; Asplund et al. 2009; Amarsi et al. 2015). In Fig. 2 we show these C I and O I spectral lines in five representative primaries, all of them with solar metallicity but covering different spectral types. We can see that the lines become very weak for the cooler stars, and the C I $\lambda 5380$ Å line may present an unknown blend for $T_{\text{eff}} < 5200$ K (Delgado Mena et al. 2021).

The line list used for the Sc, V, Mn, and Co abundances is the same as in Paper I. Table 1 lists the atomic data for the lines analysed, retrieved from the Vienna Atomic Line Database (VALD3, Ryabchikova et al. 2015).

In order to calculate the required abundances, we assumed the stellar parameters derived with STEPAR in Paper I and used the EW method, a grid of MARCS stellar atmospheric models (Gustafsson et al. 2008), and the 2019 version of the code MOOG² (Snedden 1973). The EW were computed using ARES³ (Sousa et al. 2015). The final abundances were computed in a differential manner, in a line-by-line basis, with respect to our solar spectrum (using the asteroid Vesta)

as in Paper I, which minimise systematic uncertainties that may arise due to the analysis method and atomic data used. Out of 179 stars with available stellar parameters, we measured C abundances for 161 stars, O abundances for 173 stars, Sc abundances for all 179 stars, V abundances for 176 stars, Mn abundances for all 179 stars, and Co abundances for 178 stars. Since the C I line at 5380.34 Å presents an unknown blend, it was not considered for the final carbon abundance for stars with $T_{\text{eff}} < 5200$ K. The solar abundances for each line are listed in Table 1.

The odd-Z iron-peak elements Sc, V, Mn, and Co suffer from hyperfine structure, which splits their absorption lines into multiple components (Jofré et al. 2017; Heiter et al. 2021). Shan et al. (2021) showed that the impact of hyperfine structure on certain absorption lines in cool photospheres can be more pronounced compared to Sun-like stars. Therefore, it must be considered in order to derive precise abundances with the EW method. In our analysis, we used the ‘abfind’ driver within MOOG to derive carbon and oxygen abundances. However, to account for the HFS components of Sc, V, Mn, and Co, we used the ‘blends’ driver, as in several previous studies (see e.g. da Silva et al. 2015; Maldonado et al. 2015, 2020; Biazzo et al. 2015, 2022).

Furthermore, some of the O, Mn and Co lines used in the abundance determination are affected by NLTE. Since the MARCS models are based on a standard LTE approximation, the O abundances were later corrected for NLTE effects with the corrections given by Bergemann et al. (2021), the Mn abundances with corrections by Bergemann et al. (2019), and the Co abundances with corrections by Bergemann et al. (2010) and collisional data from Voronov et al. (2022), using the web interface at <http://nlte.mpia.de/>. These corrections are based on the plane-parallel 1D MAFAGS-OS model atmosphere code (Grupp 2004). We display the NLTE corrections against the stellar parameters in Fig. 3. We found a significant trend with T_{eff} , which is positive for Mn and Co NLTE corrections but negative for O NLTE corrections. According to Zhao et al. (2016), Sc only presents large NLTE corrections in the low-metallicity regime ($[\text{Fe}/\text{H}] < -1.5$). We also compile the number of HFS components and the NLTE corrections in Table 1. The atomic data of the HFS components are compiled in Tables A2–A5.

2.3 Abundance uncertainties

In Paper I, the abundance uncertainties were computed as the scatter of the abundances obtained from each line for the same atomic species. In this work, we proceeded as in Battistini & Bensby (2015) (hereafter BB15), Delgado Mena et al. (2021) (hereafter DM21), and others, taking the uncertainties in the stellar parameters (T_{eff} , $\log g$, ξ , and $[\text{Fe}/\text{H}]$) into consideration. The abundance uncertainty due to the errors on stellar parameters were estimated by calculating the abundance differences when one of each of the stellar parameters was modified by its individual error given in Table B.3 of Paper I. The final abundance errors are given by the quadratic sum of these individual errors and the line-to-line scatter. The average of these contributions to the total uncertainty for each abundance and spectral type is given in Table 2. As the analysis is differential relative to the Sun in a line-by-line basis, systematic errors should be minimised.

Oxygen and carbon can form several molecules, such as the CO, in the atmospheres of late-type stars. Therefore, abundances of O and C are bound via chemical equilibrium. As demonstrated by Pavlenko et al. (2019), the interdependence of these abundances in solar-type stars is negligible, within the errorbars.

² <https://www.as.utexas.edu/~chris/moog.html>

³ <https://github.com/sousasag/ARES>

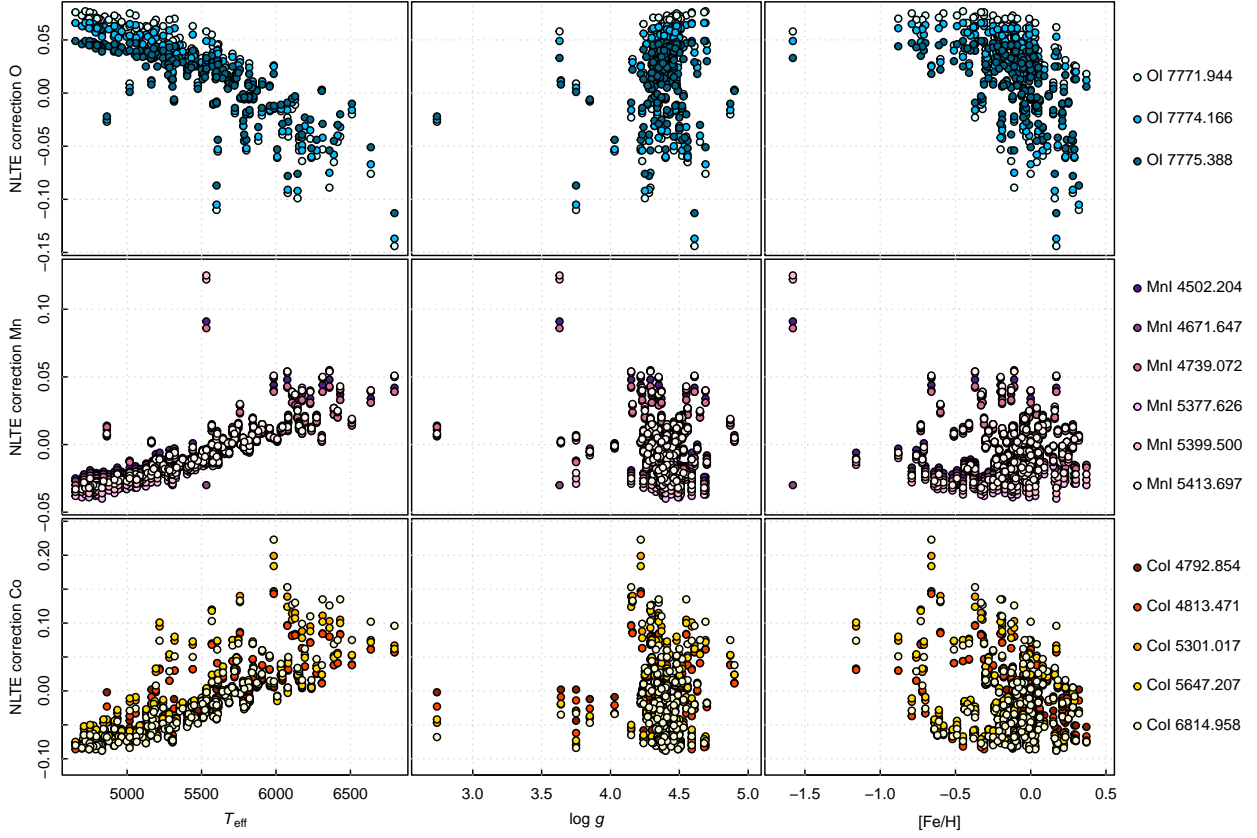


Figure 3. NLTE corrections for the O, Mn and Co lines versus de stellar parameters (T_{eff} , $\log g$, and $[\text{Fe}/\text{H}]$).

Table 2. Average of the different contributions to the total abundance uncertainties, analysing the abundance sensitivities to changes of each stellar parameter.

Abundance	Stars	Line-to-line scatter (dex)	ΔT_{eff} (dex)	$\Delta[\text{Fe}/\text{H}]$ (dex)	$\Delta \log g$ (dex)	$\Delta \xi$ (dex)	Total error (dex)
[C/H]	F-type stars	± 0.034	± 0.018	± 0.001	∓ 0.026	± 0.001	± 0.048
	G-type stars	± 0.081	± 0.023	± 0.001	∓ 0.027	± 0.001	± 0.092
	K-type stars	± 0.111	± 0.062	± 0.002	∓ 0.066	± 0.001	± 0.143
[O/H]	F-type stars	± 0.060	± 0.024	± 0.001	∓ 0.015	± 0.005	± 0.073
	G-type stars	± 0.073	± 0.034	± 0.001	∓ 0.016	± 0.003	± 0.098
	K-type stars	± 0.094	± 0.099	± 0.001	∓ 0.056	± 0.004	± 0.144
[Sc/H]	F-type stars	± 0.083	± 0.009	± 0.004	∓ 0.023	± 0.006	± 0.098
	G-type stars	± 0.075	± 0.008	± 0.004	∓ 0.022	± 0.006	± 0.089
	K-type stars	± 0.133	± 0.023	± 0.008	∓ 0.042	± 0.018	± 0.153
[V/H]	F-type stars	± 0.163	± 0.031	± 0.001	∓ 0.003	± 0.001	± 0.173
	G-type stars	± 0.065	± 0.036	± 0.000	∓ 0.000	± 0.002	± 0.079
	K-type stars	± 0.057	± 0.098	± 0.001	∓ 0.010	± 0.027	± 0.126
[Mn/H]	F-type stars	± 0.113	± 0.020	± 0.001	∓ 0.001	± 0.002	± 0.116
	G-type stars	± 0.089	± 0.020	± 0.001	∓ 0.001	± 0.006	± 0.095
	K-type stars	± 0.097	± 0.034	± 0.006	∓ 0.006	± 0.018	± 0.107
[Co/H]	F-type stars	± 0.066	± 0.023	± 0.001	∓ 0.000	± 0.001	± 0.077
	G-type stars	± 0.056	± 0.016	± 0.002	∓ 0.009	± 0.003	± 0.061
	K-type stars	± 0.074	± 0.012	± 0.008	∓ 0.038	± 0.011	± 0.087

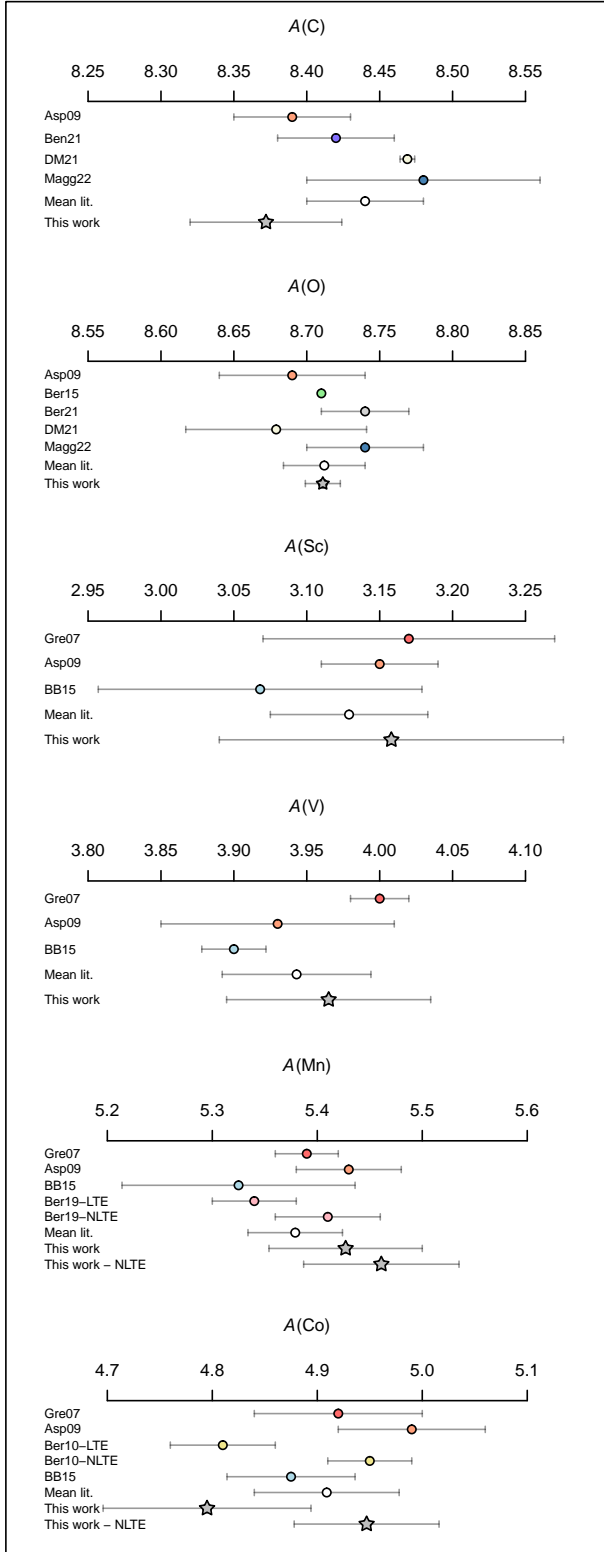


Figure 4. Comparison for our solar abundances (gray stars) with the literature: Grevesse et al. (2007) (Gre07 – red), Asplund et al. (2009) (Asp09 – orange), Bergemann et al. (2010) (Ber10 – yellow), Bertran de Lis et al. (2015) (Ber15 – green), Battistini & Bensby (2015) (BB15 – blue), Bergemann et al. (2019) (Ber19 – pink), Bensby et al. (2021) (Ben21 – purple), Bergemann et al. (2021) (Ber21 – light gray), Delgado Mena et al. (2021) (DM21 – beige), Magg et al. (2022) (Magg22 – dark blue), and the mean value from the literature (Mean lit. – white).

2.4 Solar abundances

Since our analysis is differential relative to the Sun in a line-by-line basis, we also derived the abundances for the Sun, obtaining $A(\text{C})_{\odot} = 8.372 \pm 0.052$ dex, $A(\text{O})_{\odot} = 8.711 \pm 0.012$ dex, $A(\text{Sc})_{\odot} = 3.158 \pm 0.118$ dex, $A(\text{V})_{\odot} = 3.965 \pm 0.070$ dex, $A(\text{Mn})_{\odot} = 5.427 \pm 0.073$ dex, and $A(\text{Co})_{\odot} = 4.795 \pm 0.099$ dex. The comparison between our solar abundances and the ones from the literature is shown in Fig. 4. The differences may be due to the use of different line lists, and the assumptions made, such as LTE, 1D models, etc.

3 RESULTS AND DISCUSSION

3.1 Carbon and oxygen abundances

We display the distributions of $[\text{C}/\text{Fe}]$, $[\text{O}/\text{Fe}]$, and $[\text{C}/\text{O}]$ as a function of metallicity in left panels of Fig. 5. Previous papers (e.g. Bertran de Lis et al. 2015, DM21) have set the limit for reliable abundances of C and O at 5200 K; for stars below this effective temperature, abundances provided by different lines start to disagree. In Fig. 5 we distinguish stars with $T_{\text{eff}} < 5200$ K as open circles, and note that most of the outliers belong to this category. Our analysis revealed increasing $[\text{C}/\text{Fe}]$ and $[\text{O}/\text{Fe}]$ ratios with decreasing $[\text{Fe}/\text{H}]$, while the $[\text{C}/\text{O}]$ ratio increase towards higher metallicities. Moreover, adopting the Galactic populations derived in Paper I from the Galactocentric space velocities (see Montes et al. 2001; Bensby et al. 2003, 2005), namely halo, thick disc, thick-to-thin transition disc, and thin disc, we observed that thick disc stars present higher $[\text{C}/\text{Fe}]$ and $[\text{O}/\text{Fe}]$ values than thin disc stars in the common metallicity interval. Furthermore, we overplot (with orange lines) the GCE models from Kobayashi et al. (2020) (hereafter K20 model), which assumed failed supernovae (SNe) for stars with initial masses higher than $30M_{\odot}$. For the $[\text{O}/\text{Fe}]$ abundance we also included a K20 model without failed SNe. To better examine the trends of these ratios with increasing metallicity, we show box and whisker plots in right panels of Fig. 5.

Our findings on the $[\text{C}/\text{Fe}]$ trend are consistent with previous studies by Delgado Mena et al. (2010, 2021) and Amarsi et al. (2019). Other authors reported similar results (e.g. Takeda & Honda 2005; Reddy et al. 2006; González Hernández et al. 2010, 2013; Nissen et al. 2014; Buder et al. 2019; Franchini et al. 2020; Stonkutė et al. 2020), showing increasing $[\text{C}/\text{Fe}]$ ratios with decreasing metallicity down to $[\text{Fe}/\text{H}] \sim -0.8$ dex, after which the trend flattens and then decreases for halo stars. Notably, the halo star HD 149414 Aa,Ab exhibits a higher carbon abundance than expected based on the general trend. This overabundance could be attributed to the fact that this star is a single-lined spectroscopic binary (SB1; Latham et al. 2002) with $T_{\text{eff}} = 5217 \pm 57$ K, in close proximity to the 5200 K limit.

Several studies have examined the distribution of $[\text{O}/\text{Fe}]$ over $[\text{Fe}/\text{H}]$, and found that the $[\text{O}/\text{Fe}]$ ratio rises with decreasing metallicity, albeit with varying slopes, and reaches a plateau around $[\text{Fe}/\text{H}] = -0.8$ dex. While some of them found just a shallow decline in the $[\text{O}/\text{Fe}]$ trend at high metallicities (e.g. Bensby et al. 2004, 2014; Takeda & Honda 2005; Ramírez et al. 2007; Petigura & Marcy 2011; Franchini et al. 2021), other studies suggested a flattening at solar or super-solar metallicities (e.g. Bensby et al. (2004); Ramírez et al. (2013); Bertran de Lis et al. (2015), DM21). These differences could be attributed to the use of different oxygen indicators or whether the author included or neglected NLTE effects, inelastic collisions with hydrogen, etc. In this case, the red giant branch star BD+80 245 ($[\text{Fe}/\text{H}] = -1.58 \pm 0.07$ dex) shows a low O abundance when compared to the Galactic trend. The low metallicity, which implies weak lines, and low signal-to-noise ratio of this star ($\text{S/N} \sim 60$)

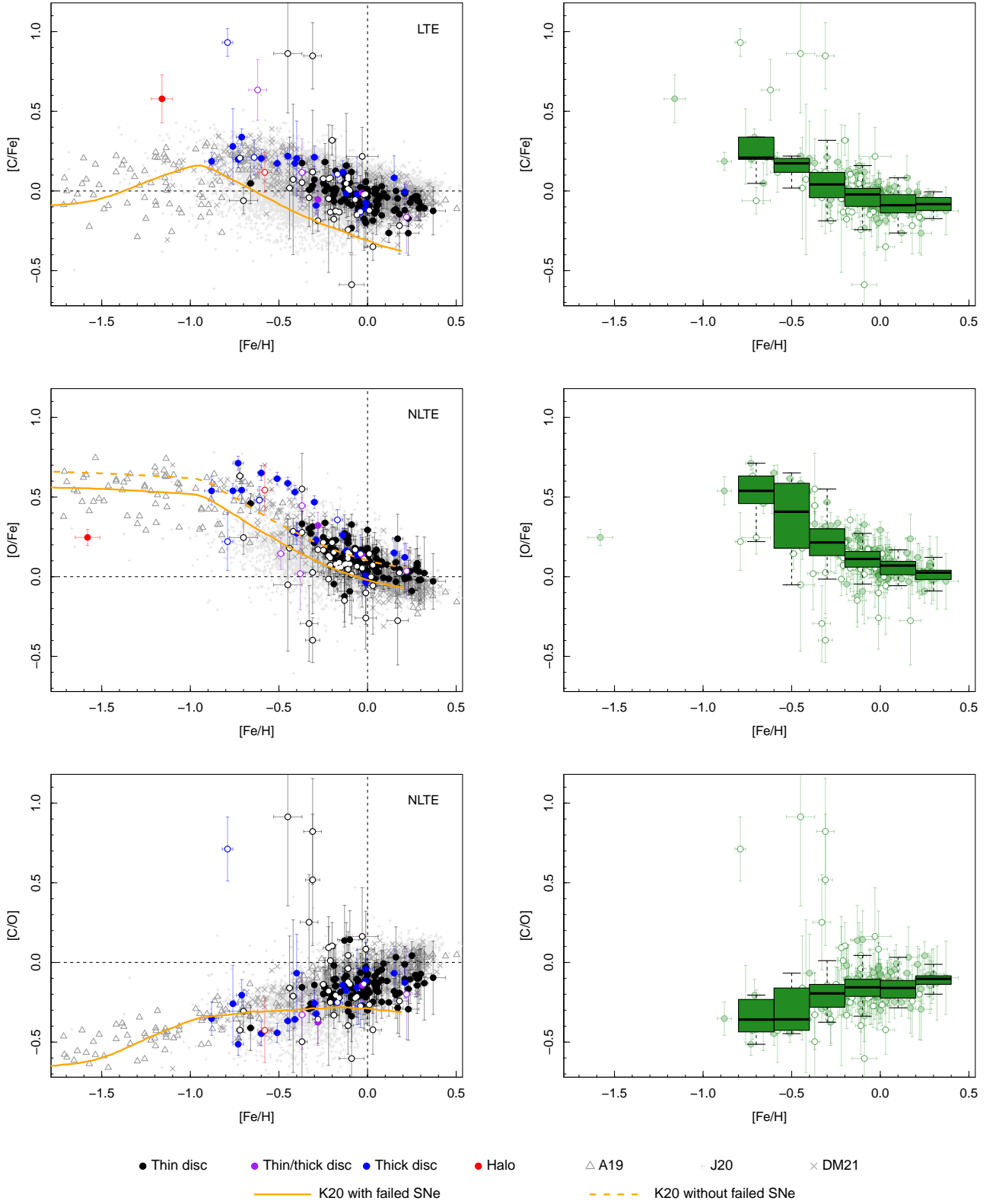


Figure 5. Left panels: Abundance ratios of $[C/Fe]$, $[O/Fe]$, and $[C/O]$ versus $[Fe/H]$, in comparison with [Amarsi et al. \(2019\)](#) (A19) using the 1D/NLTE results, [Jönsson et al. \(2020\)](#) (J20), and [DM21](#). Colours for different populations: black – thin disc, blue – thick disc, purple – thin/thick disc, red – halo. Open circles: stars with $T_{\text{eff}} < 5200$ K; filled circles: stars with $T_{\text{eff}} \geq 5200$ K. Models of GCE from [Kobayashi et al. \(2020\)](#) with failed SNe at $> 30M_{\odot}$ (solid orange line) and without failed SNe (dotted orange line) are overplotted. Right panels: Box and whisker plots of $[C/Fe]$, $[O/Fe]$, and $[C/O]$ versus $[Fe/H]$.

could explain the underabundance obtained with the EW method. Moreover, we note that the thick-disc stars present higher C and O abundances than the thin-disc stars at equivalent $[\text{Fe}/\text{H}]$ values.

These results for the $[\text{C}/\text{Fe}]$ and $[\text{O}/\text{Fe}]$ trends discussed above are consistent with what is expected from Galactic chemical evolution. Both $[\text{C}/\text{Fe}]$ and $[\text{O}/\text{Fe}]$ decrease with increasing $[\text{Fe}/\text{H}]$, which reflects the increasing relevance of SNe Ia with time, fueling the increase in iron, relative to SNe II. However, the slopes of both trends are different, with the carbon following iron more closely than oxygen, due to their different production sites. Oxygen is produced by SNe II from massive progenitors (Woosley & Weaver 1995). Carbon, on the other hand, is produced by synthesis in stellar interiors, then dredged up from cores and released into the interstellar medium by massive stellar winds and radiation pressure (Gustafsson et al. 1999). However, the lower-mass post-AGB stars contribute as well, and their relative importance is still a matter of debate (see Franchini et al. 2020, and references therein). Therefore, the enrichment of carbon is delayed in time with respect to oxygen, explaining the different slopes. As can be seen in Fig. 5, our results follow the general trend of the K20 models but, as stated by Kobayashi et al. (2020), the predicted $[\text{C}/\text{Fe}]$ is ~ 0.1 – 0.2 dex lower than the observational data, with a steeper decrease for $[\text{Fe}/\text{H}] > -1$. However, as shown by Delgado Mena et al. (2021) in their Fig. 3, including the contribution of Wolf–Rayet stars to the carbon production can increase the $[\text{C}/\text{Fe}]$ abundance (Kobayashi et al. in prep.). In the case of $[\text{O}/\text{Fe}]$, the model follows the general trend of the observations, but with lower abundances for $[\text{Fe}/\text{H}] > -1$ dex. In this case, we also added a K20 model without failed SNe (dashed orange line), which seems to better reproduce our results for $[\text{Fe}/\text{H}] > -1$ dex.

In the upper panel of Fig. 6 we compare the $[\text{C}/\text{H}]$ and $[\text{O}/\text{H}]$ ratios for the five stars in common with DM21. DM21 provide the abundances of the O I 6158 and 6300 Å lines independently, hence we represent our O abundances (using the O I infrared triplet) against both results. The abundances of these stars closely correspond to those provided by DM21, especially in the case of carbon abundances, which exhibit a low scatter.

3.2 Odd-Z iron-peak abundances

We show the distribution of $[\text{X}/\text{Fe}]$ ratios for the odd-Z iron-peak elements versus the metallicity in Fig. 7, in comparison with the results of BB15. We also overplot in orange a modification of the GCE models from Kobayashi et al. (2011) that includes a hypernova jet effect (dashed line; hereafter K15, see Sneden et al. 2016; Zhao et al. 2016; Kobayashi et al. 2020), and the K20 models (solid line). The $[\text{Sc}/\text{Fe}]$ vs. $[\text{Fe}/\text{H}]$ trend behave like the α -elements, which suggests a common production site, and it is in good agreement with the results by Nissen et al. (2000), Brewer & Carney (2006), Neves et al. (2009), Adibekyan et al. (2012b), Tabernero et al. (2012), and BB15. We observe higher abundances for the thick disc stars in contrast to the thin disc. The K20 model predicts $[\text{Sc}/\text{Fe}] \sim -1$ dex for our metallicity range, not visible in our panel. The K15 model provides a better fit to the observations, though it does not show the weak decrease of $[\text{Sc}/\text{Fe}]$ with increasing metallicity for $[\text{Fe}/\text{H}] > -1$ dex. In theoretical models, both Sc and V are consistently found to be underproduced across all metallicity ranges compared to observational data. The abundances of both elements could potentially be influenced by the neutrino process, a factor not accounted for in these GCE models.

The $[\text{V}/\text{Fe}]$ vs. $[\text{Fe}/\text{H}]$ trend also emulates an α -element, with solar abundance at $[\text{Fe}/\text{H}] = 0$ and a rise towards lower metallicities, but with significantly more scatter than the other elements when

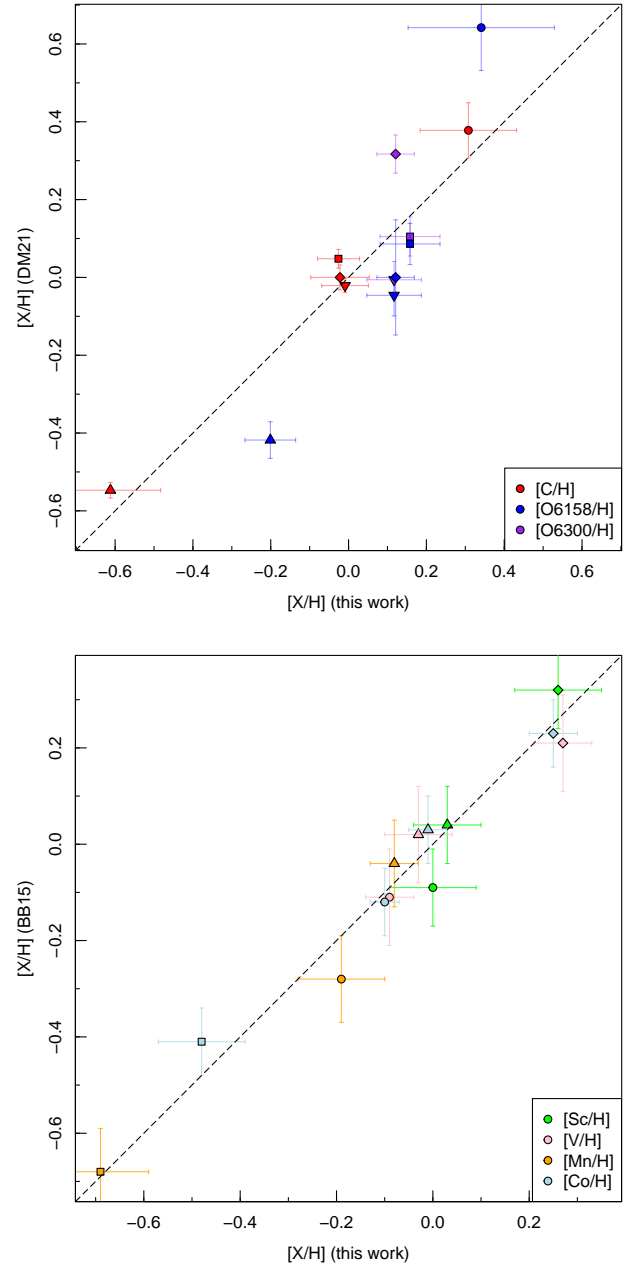


Figure 6. Upper panel: Comparison between the C and O abundances obtained by DM21 (who reported the O I 6158 and 6300 Å abundances independently), and by this work for the stars in common: HD 8389 A (circle), HD 11964 A (square), HD 40397 A (diamond), HD 59984 (point-up triangle), and HD 222582 A (point-down triangle). Lower panel: Comparison between the Sc, V, Mn, and Co abundances by BB15 and by this work, only in LTE, for the stars in common: HD 40397 A (circle), HD 114606 A (square), HD 190360 A (diamond), and HD 222582 A (point-up triangle).

including the stars with $T_{\text{eff}} < 5200$ K. Vanadium is an intricate element that presents biases and higher dispersion for the cooler objects. For this reason, some studies established a cutoff limit around 5300 K (for example, see Neves et al. 2009 and Adibekyan et al. 2012b). The general trend is consistent with Brewer & Carney (2006), Neves et al. (2009), Adibekyan et al. (2012b), Tabernero et al. (2012), and BB15. As in the case of Sc, V is underproduced by the GCE models. The K20 model shows a plateau and a weak decrease toward

higher metallicities for $[\text{Fe}/\text{H}] > -1$ dex, a similar behaviour that the observations, despite the 0.4–0.5 dex bias.

The $[\text{Mn}/\text{Fe}]$ vs. $[\text{Fe}/\text{H}]$ trend, assuming LTE, seems to work opposite to an α -element (Gratton 1989), i.e. it decreases steadily towards lower metallicities and shows sub-solar abundances for all metallicities up to $[\text{Fe}/\text{H}] = 0$. This trend can be explained by models in which Mn is produced in SNII at metallicities below $[\text{Fe}/\text{H}] < -1$ (Tsujiimoto & Shigezuma 1998), while at $[\text{Fe}/\text{H}] > -1$ the increasing $[\text{Mn}/\text{Fe}]$ ratio with increasing $[\text{Fe}/\text{H}]$ is due to a contribution from SNIa (Kobayashi 2016). This trend is in good agreement with the results by Nissen et al. (2000), Brewer & Carney (2006), Feltzing et al. (2007), Neves et al. (2009), Adibekyan et al. (2012b), Taberner et al. (2012), and BB15. Nonetheless, when taking into account NLTE corrections, our trend presents a different behaviour compared to the one by BB15, whose trend becomes virtually flat over the metallicity range studied. As the authors discussed, no models have been able to explain this flattening. The K20 model predicts a plateau around $[\text{Mn}/\text{Fe}] \sim 0.55$ dex for the low-metallicity regime, and then an increase above $[\text{Fe}/\text{H}] > -1$ dex.

Co shows a trend similar to α -elements, with over-abundant $[\text{Co}/\text{Fe}]$ at low metallicities. The halo star BD+80 245 (G0 IV) seems to be Co-rich. Assuming LTE, this trend is in agreement with Brewer & Carney (2006), Neves et al. (2009), Adibekyan et al. (2012b), Taberner et al. (2012), and BB15. However, we find some differences when considering NLTE corrections in comparison with BB15, who reported higher Co abundances for a given metallicity. The K20 model reproduces the α -element trend, but provides values ~ 0.3 dex lower than the observations. However, when including the hypernova jet effects (K15 model), the prediction is closer to the data.

Since our results for Mn and Co abundances assuming LTE are in good agreement with those by BB15, the differences when considering NLTE seem to be due to the use of different NLTE corrections. We compared our results of the $[\text{Sc}/\text{H}]$, $[\text{V}/\text{H}]$, $[\text{Mn}/\text{H}]$, and $[\text{Co}/\text{H}]$ ratios for the four stars in common with BB15 in the lower panel of Fig. 6, finding similar values.

Finally we compared these results with the ones obtained in Paper I without taking into account the HFS and NLTE effects in Fig. 8. We found that the outliers with $[\text{Sc}/\text{Fe}] > 0.5$ disappear and the stars now follow the general Galactic trend, but the halo star BD+80 245 (G0 IV), which presents a lower Sc abundance. Regarding the V abundances, the new results exhibit reduced scatter, with the persistent outliers attributed to lower effective temperatures, below 5200 K. When accounting for HFS and NLTE, we generally observed slightly higher Mn abundances and some diminished Co abundances, while maintaining the same overall trend.

3.3 Exoplanets

Analysing the correlations between stellar properties, such as metallicity and chemical abundances, and the occurrence of exoplanets can provide valuable insights for the selection of targets in forthcoming exoplanet surveys and for comprehending the mechanisms behind planetary formation. In particular, it has been extensively reported that the stars that host giant planets present higher metallicities than the stars without detected planets (e.g. Gonzalez 1997; Fischer & Valenti 2005; Brewer et al. 2016). This giant planet – stellar metallicity correlation supports the core-accretion scenario as the basis for planet formation (e.g. Ida & Lin 2004; Ercolano & Clarke 2010). The main goal of this section is to examine potential notable distinctions between the sample of stars hosting planets and the sample of stars lacking known planets, specifically regarding metals aside from iron.

We conducted a search for confirmed exoplanets around the primary stars of our sample in the literature using The Extrasolar Planets Encyclopaedia⁴. In Paper I, 21 exoplanets in 14 planetary systems were found in the literature; now we have 24 exoplanets in 17 planetary systems. Two exoplanets were originally listed for the star HD 38529 A in Paper I, but it has since been determined that one of them is a substellar companion of $23.7^{+4.1}_{-3.1} M_{\text{Jup}}$. As a result, we now recognise only one exoplanet orbiting this star. Moreover, none of the M-dwarf companions in our sample present confirmed exoplanets. We plot in Fig. 9 the galactic trends for $[\text{C}/\text{Fe}]$, $[\text{O}/\text{Fe}]$, and $[\text{C}/\text{O}]$, indicating the stars with confirmed exoplanets with $m \sin i$ greater or less than 30 Earth masses ($\sim 0.094 M_{\text{Jup}}$), in comparison to single stars. As discussed in Paper I, the exoplanet host stars tend to be metal-rich. Given the small number of exoplanet host stars in our sample, we do not see any difference between the stars harboring exoplanets with $m \sin i$ greater or less than 30 Earth masses.

In Paper I we performed a Kolmogorov-Smirnov (K-S) test to evaluate the disparity between the stars in our sample with and without planets, independently of their mass, safely concluding that both metallicity distributions were significantly different. Now we repeated the K-S test for the $[\text{Fe}/\text{H}]$, since the number of known exoplanet has increased, but we obtain the same results. The probability that both samples follow the same distribution is just of 0.0004. We compile the K-S statistics and p -values in Table 3, and plot the corresponding cumulative distribution function in Fig. 10. The p -value represents the significance level of the K-S test, i.e. the probability that the two groups belong to the same population.

Preceding studies indicated that planet hosts and single stars seem to be evenly distributed for solar metallicity, and the presence of planets does not lead to differences in the carbon abundances. However, for sub-solar metallicities, planet hosts present an enhancement of C (see Nissen et al. 2014; Delgado Mena et al. 2021). We applied the K-S test for the $[\text{C}/\text{Fe}]$, $[\text{O}/\text{Fe}]$, and $[\text{C}/\text{O}]$ ratios, finding that only for the $[\text{C}/\text{Fe}]$ ratio, the distributions of host and single stars are different, with only a probability of 0.0242 that both populations have the same $[\text{C}/\text{Fe}]$ distribution. These results are in agreement with da Silva et al. (2015) and Delgado Mena et al. (2021), who showed a significant difference in carbon abundance between host and single stars, but no difference, or not so strong, in the case of oxygen.

Repeating the analysis for the $[\text{X}/\text{Fe}]$ ratios of the odd-Z iron-peak elements, we obtained that only for the $[\text{Mn}/\text{Fe}]$ ratio, both distributions are significantly different, with just a probability of 0.0023 for the planet hosts and single stars of coming from the same distribution. Previous studies reported overabundances of $[\text{Mn}/\text{Fe}]$ of planet hosts in comparison to single stars (Zhao et al. 2002; Bodaghee et al. 2003; Kang et al. 2011; da Silva et al. 2015). Nevertheless, Adibekyan et al. (2012a) did not find that difference for the $[\text{Mn}/\text{Fe}]$ ratio.

Our findings might indicate that other species than iron also play an important role in the planet formation mechanisms; for example, carbon is a pivotal element in the formation of ices within a protoplanetary disc. The overabundance of Mn could be explained by its lower condensation temperature in comparison to the other investigated elements. Notwithstanding, these results should be revised in the future with a larger sample of exoplanet hosts.

⁴ <http://exoplanet.eu>

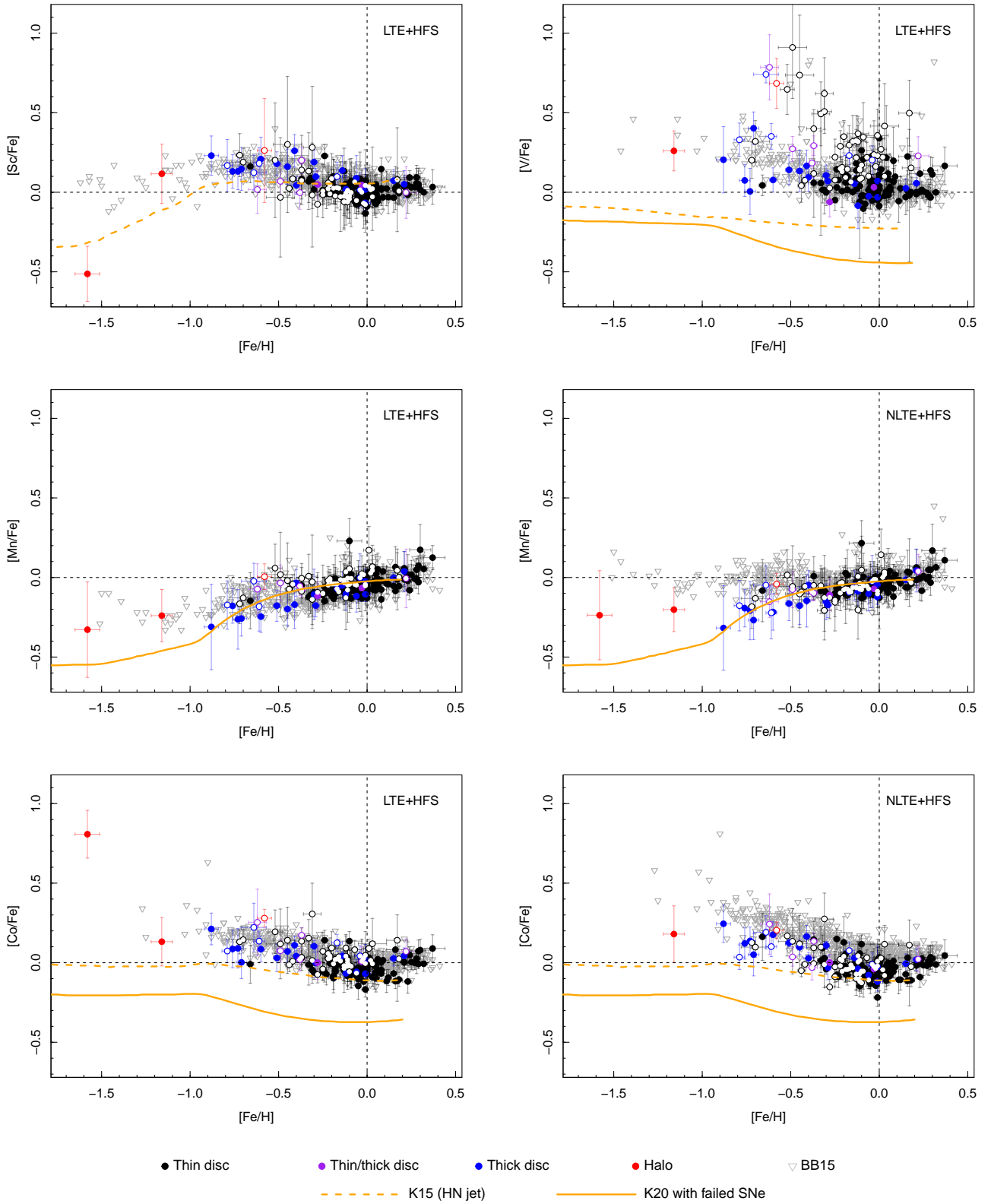


Figure 7. Abundance ratios of [Sc/Fe], [V/Fe], [Mn/Fe] (LTE and NLTE), and [Co/Fe] (LTE and NLTE) versus [Fe/H], in comparison with BB15. Colours for different populations: black – thin disc, blue – thick disc, cyan – thin/thick disc, red – halo. Open circles: stars with $T_{\text{eff}} < 5200$ K; filled circles: stars with $T_{\text{eff}} \geq 5200$ K. Models of GCE from Kobayashi et al. (2011), modified to include a hypernova jet effect (dotted orange line), and from Kobayashi et al. (2020) with failed SNe at $> 30M_{\odot}$ (solid orange line) are overplotted.

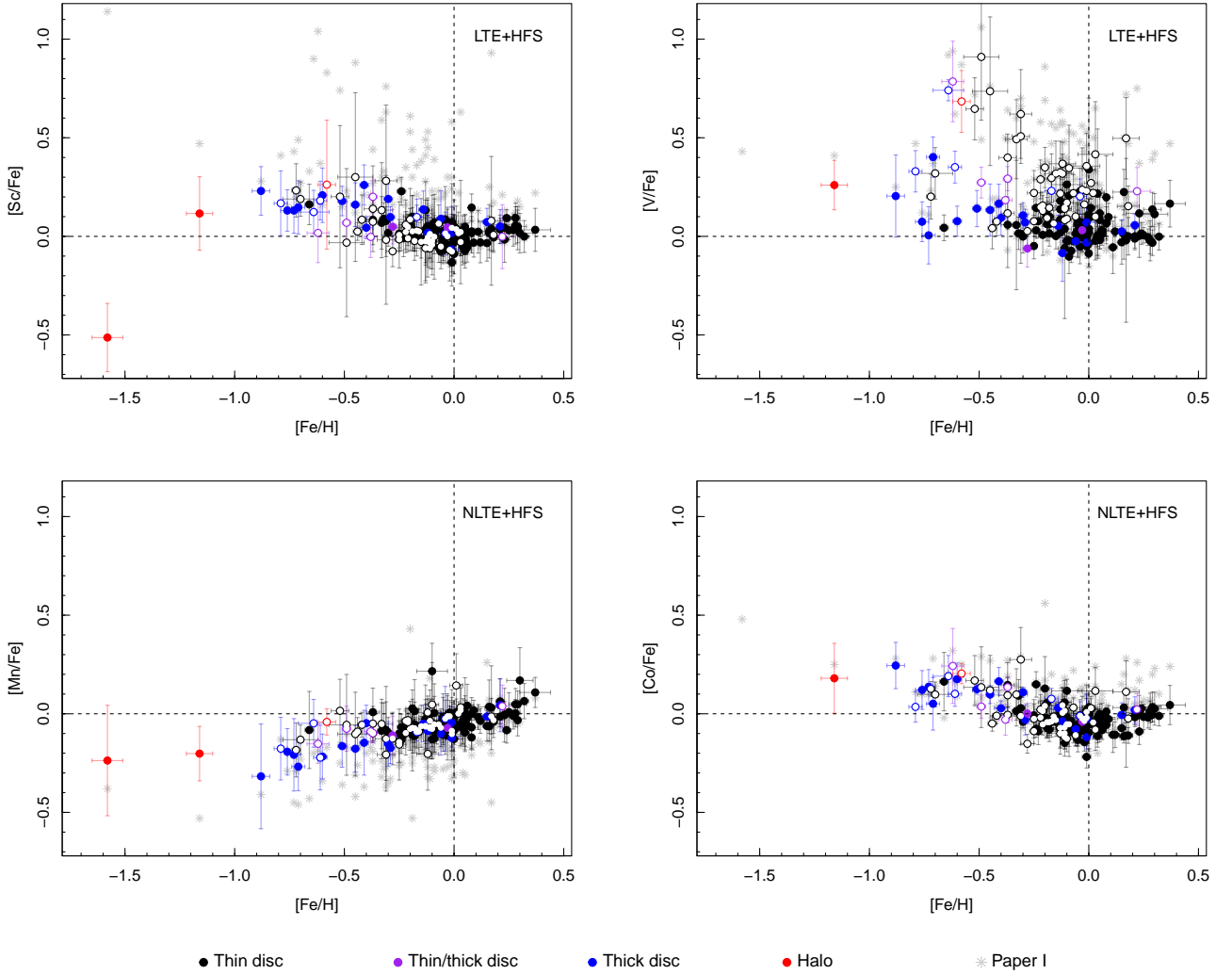


Figure 8. Abundance ratios of [Sc/Fe], [V/Fe], [Mn/Fe], and [Co/Fe] versus [Fe/H], including HFS splitting and NLTE effects when necessary, in comparison with Paper I (gray asterisks). Colours for different populations: black – thin disc, blue – thick disc, cyan – thin/thick disc, red – halo. Open circles: stars with $T_{\text{eff}} < 5200$ K; filled circles: stars with $T_{\text{eff}} \geq 5200$ K.

Table 3. Kolmogorov-Smirnoff test results

Abundance	D	p -value
[Fe/H]	0.5228	0.0004
[C/Fe]	0.3781	0.0242
[O/Fe]	0.2557	0.2496
[C/O]	0.1452	0.8763
[Sc/Fe]	0.2966	0.1545
[V/Fe]	0.2785	0.2098
[Mn/Fe]	0.4635	0.0023
[Co/Fe]	0.2313	0.3727

4 CONCLUSIONS

In this paper, we extended the analysis of the chemical abundances of FGK stars with M-dwarf companions by deriving abundances of C and O, and updating the abundances of Sc, V, Mn, and Co taking into account hyperfine structure effects and correcting for non-local thermodynamic equilibrium. For that, we made use of the equivalent

width method and high-resolution spectra. We compared our results with previous abundance determinations of F-, G-, and K-dwarfs found in the literature, finding a good agreement in the Galactic trends of the investigated abundances. As in previous studies, we noticed that some of the obtained abundances are not reliable for stars with $T_{\text{eff}} < 5200$ K, especially C, O, and V. Furthermore, we analysed the abundances of stars with and without known exoplanets and found that only for C and Mn abundances, these two populations show statistical difference.

The findings from this ongoing series devoted to investigate the metallicity and abundances of M-type dwarf stars through the use of wide physical binary systems will be beneficial for forthcoming research on the abundance of M dwarfs, which has been an expanding area of study in recent years. For instance, Abia et al. (2020) focused on the abundance of Rb, Zr and Sr of M dwarfs, while Shan et al. (2021) examined V abundance, and Tabernero et al. (in prep.) explored the rock-forming elements Mg and Si. All three studies utilised CARMENES data. Upcoming papers in this series will focus on the calibration of spectral indices from low-resolution spectra of M-dwarf companions to match the chemical composition of their

primary stars (see [Alonso-Floriano et al. 2015](#)). Additionally, we will use CARMENES high-resolution spectra to derive stellar atmospheric parameters and abundances of the M-dwarf companions through spectral synthesis. These abundances will then be compared against those presented here and [Paper I](#) for the primary stars. By providing accurate determinations of chemical abundances in M dwarfs, this series of papers will prove invaluable for future research.

ACKNOWLEDGEMENTS

We thank the anonymous referee for their comments and suggestions, which improved our manuscript. This work has made use of the NASA's Astrophysics Data System; the Washington Double Star catalogue maintained at the U.S. Naval Observatory; the VALD database, operated at Uppsala University, the Institute of Astronomy RAS in Moscow, and the University of Vienna; the portal [exoplanet.eu](#) of The Extrasolar Planets Encyclopaedia; and data from the European Space Agency (ESA) mission *Gaia*. We acknowledge financial support from the Universidad Complutense de Madrid and the Agencia Estatal de Investigación (AEI/10.13039/501100011033) of the Ministerio de Ciencia e Innovación and the ERDF "A way of making Europe" through projects PID2019-109522GB-C5[1,4] and PID2022-137241NB-C4[2,4].

DATA AVAILABILITY

The data in Table A1 are available via CDS.

REFERENCES

- Abia C., et al., 2020, *A&A*, **642**, [A227](#)
 Abt A., 1952, *ApJ*, **115**, [199](#)
 Adams F. C., Laughlin G., 1997, *Reviews of Modern Physics*, **69**, [337](#)
 Adibekyan V. Z., et al., 2012a, *A&A*, **543**, [A89](#)
 Adibekyan V. Z., Sousa S. G., Santos N. C., Delgado Mena E., González Hernández J. I., Israelian G., Mayor M., Khachatryan G., 2012b, *A&A*, **545**, [A32](#)
 Allard F., Hauschildt P. H., Schwenke D., 2000, *ApJ*, **540**, [1005](#)
 Alonso-Floriano F. J., et al., 2015, *A&A*, **577**, [A128](#)
 Amarsi A. M., Asplund M., Collet R., Leenaarts J., 2015, *MNRAS*, **454**, [L11](#)
 Amarsi A. M., Nissen P. E., Skúladóttir Á., 2019, *A&A*, **630**, [A104](#)
 Asplund M., Grevesse N., Sauval A. J., Scott P., 2009, *ARA&A*, **47**, [481](#)
 Bahcall J. N., Soneira R. M., 1980, *ApJS*, **44**, [73](#)
 Baraffe I., Chabrier G., Allard F., Hauschildt P. H., 1998, *A&A*, **337**, [403](#)
 Battistini C., Bensby T., 2015, *A&A*, **577**, [A9](#)
 Bean J. L., Sneden C., Hauschildt P. H., Johns-Krull C. M., Benedict G. F., 2006, *ApJ*, **652**, [1604](#)
 Bensby T., Feltzing S., Lundström I., 2003, *A&A*, **410**, [527](#)
 Bensby T., Feltzing S., Lundström I., 2004, *A&A*, **415**, [155](#)
 Bensby T., Feltzing S., Lundström I., Ilyin I., 2005, *A&A*, **433**, [185](#)
 Bensby T., Feltzing S., Oey M. S., 2014, *A&A*, **562**, [A71](#)
 Bensby T., et al., 2021, *A&A*, **655**, [A117](#)
 Bergemann M., Pickering J. C., Gehren T., 2010, *MNRAS*, **401**, [1334](#)
 Bergemann M., et al., 2019, *A&A*, **631**, [A80](#)
 Bergemann M., et al., 2021, *MNRAS*, **508**, [2236](#)
 Bertran de Lis S., Delgado Mena E., Adibekyan V. Z., Santos N. C., Sousa S. G., 2015, *A&A*, **576**, [A89](#)
 Biazzo K., et al., 2015, *A&A*, **583**, [A135](#)
 Biazzo K., et al., 2022, *A&A*, **664**, [A161](#)
 Bodaghee A., Santos N. C., Israelian G., Mayor M., 2003, *A&A*, **404**, [715](#)
 Bond J. C., O'Brien D. P., Laretta D. S., 2010, *ApJ*, **715**, [1050](#)
 Brewer M.-M., Carney B. W., 2006, *AJ*, **131**, [431](#)
 Brewer J. M., Fischer D. A., Valenti J. A., Piskunov N., 2016, *ApJS*, **225**, [32](#)
 Buder S., et al., 2019, *A&A*, **624**, [A19](#)
 Burrows A., et al., 1997, *ApJ*, **491**, [856](#)
 Carter-Bond J. C., O'Brien D. P., Raymond S. N., 2012, *ApJ*, **760**, [44](#)
 Chabrier G., 2003, *PASP*, **115**, [763](#)
 Delgado Mena E., Israelian G., González Hernández J. I., Bond J. C., Santos N. C., Udry S., Mayor M., 2010, *ApJ*, **725**, [2349](#)
 Delgado Mena E., Adibekyan V., Santos N. C., Tsantaki M., González Hernández J. I., Sousa S. G., Bertrán de Lis S., 2021, *A&A*, **655**, [A99](#)
 Des Marais D. J., et al., 2002, *Astrobiology*, **2**, [153](#)
 Draine B. T., Li A., 2007, *ApJ*, **657**, [810](#)
 Duque-Arribas C., Montes D., Tabernero H. M., Caballero J. A., Gorgas J., Marfil E., 2023, *ApJ*, **944**, [106](#)
 Ercolano B., Clarke C. J., 2010, *MNRAS*, **402**, [2735](#)
 Feltzing S., Fohlman M., Bensby T., 2007, *A&A*, **467**, [665](#)
 Ferguson D., Gardner S., Yanny B., 2017, *ApJ*, **843**, [141](#)
 Fischer D. A., Valenti J., 2005, *ApJ*, **622**, [1102](#)
 Franchini M., et al., 2020, *ApJ*, **888**, [55](#)
 Franchini M., et al., 2021, *AJ*, **161**, [9](#)
 Gaia Collaboration et al., 2022, *arXiv e-prints*, p. [arXiv:2208.00211](#)
 Gonzalez G., 1997, *MNRAS*, **285**, [403](#)
 González Hernández J. I., Israelian G., Santos N. C., Sousa S., Delgado-Mena E., Neves V., Udry S., 2010, *ApJ*, **720**, [1592](#)
 González Hernández J. I., Delgado-Mena E., Sousa S. G., Israelian G., Santos N. C., Adibekyan V. Z., Udry S., 2013, *A&A*, **552**, [A6](#)
 Gratton R. G., 1989, *A&A*, **208**, [171](#)
 Grevesse N., Asplund M., Sauval A. J., 2007, *Space Sci. Rev.*, **130**, [105](#)
 Grupp F., 2004, *A&A*, **420**, [289](#)
 Gustafsson B., Karlsson T., Olsson E., Edvardsson B., Ryde N., 1999, *A&A*, **342**, [426](#)
 Gustafsson B., Edvardsson B., Eriksson K., Jørgensen U. G., Nordlund Å., Plez B., 2008, *A&A*, **486**, [951](#)
 Heiter U., et al., 2021, *A&A*, **645**, [A106](#)
 Henry T. J., Jao W.-C., Subasavage J. P., Beaulieu T. D., Ianna P. A., Costa E., Méndez R. A., 2006, *AJ*, **132**, [2360](#)
 Ida S., Lin D. N. C., 2004, *ApJ*, **616**, [567](#)
 Ishikawa H. T., Aoki W., Kotani T., Kuzuhara M., Omiya M., Reiners A., Zechmeister M., 2020, *PASJ*, **72**, [102](#)
 Jofré P., et al., 2017, *A&A*, **601**, [A38](#)
 Jönsson H., et al., 2020, *AJ*, **160**, [120](#)
 Kang W., Lee S.-G., Kim K.-M., 2011, *ApJ*, **736**, [87](#)
 Kiseleman D., 1993, *A&A*, **275**, [269](#)
 Kobayashi C., 2016, *Nature*, **540**, [205](#)
 Kobayashi C., Karakas A. I., Umeda H., 2011, *MNRAS*, **414**, [3231](#)
 Kobayashi C., Karakas A. I., Lugaro M., 2020, *ApJ*, **900**, [179](#)
 Kopparapu R. K., Ramirez R. M., Schottelkotte J., Kasting J. F., Domagal-Goldman S., Eymet V., 2014, *ApJ*, **787**, [L29](#)
 Kurucz R. L., 1993, *Physica Scripta Volume T*, **47**, [110](#)
 Larimer J. W., 1975, *Geochimica Cosmochimica Acta*, **39**, [389](#)
 Latham D. W., Stefanik R. P., Torres G., Davis R. J., Mazeh T., Carney B. W., Laird J. B., Morse J. A., 2002, *AJ*, **124**, [1144](#)
 Leger A., Puget J. L., 1984, *A&A*, **137**, [L5](#)
 Magg E., et al., 2022, *A&A*, **661**, [A140](#)
 Maldonado J., Eiroa C., Villaver E., Montesinos B., Mora A., 2015, *A&A*, **579**, [A20](#)
 Maldonado J., et al., 2020, *A&A*, **644**, [A68](#)
 Mann A. W., Brewer J. M., Gaidos E., Lépine S., Hilton E. J., 2013, *AJ*, **145**, [52](#)
 Mann A. W., Deacon N. R., Gaidos E., Ansdell M., Brewer J. M., Liu M. C., Magnier E. A., Aller K. M., 2014, *AJ*, **147**, [160](#)
 Marboeuf U., Thiabaud A., Alibert Y., Cabral N., Benz W., 2014, *A&A*, **570**, [A36](#)
 Marfil E., et al., 2021, *A&A*, **656**, [A162](#)
 Meynet G., Maeder A., 2002, *A&A*, **390**, [561](#)
 Montes D., López-Santiago J., Gálvez M. C., Fernández-Figueroa M. J., De Castro E., Cornide M., 2001, *MNRAS*, **328**, [45](#)
 Montes D., et al., 2018, *MNRAS*, **479**, [1332](#)
 Moustakas J., Kennicutt Robert C. J., Tremonti C. A., Dale D. A., Smith J.-D. T., Calzetti D., 2010, *ApJS*, **190**, [233](#)

Neves V., Santos N. C., Sousa S. G., Correia A. C. M., Israelian G., 2009, *A&A*, 497, 563

Newton E. R., Charbonneau D., Irwin J., Berta-Thompson Z. K., Rojas-Ayala B., Covey K., Lloyd J. P., 2014, *AJ*, 147, 20

Nissen P. E., Chen Y. Q., Schuster W. J., Zhao G., 2000, *A&A*, 353, 722

Nissen P. E., Chen Y. Q., Carigi L., Schuster W. J., Zhao G., 2014, *A&A*, 568, A25

Passegger V. M., et al., 2018, *A&A*, 615, A6

Pavlenko Y. V., Kaminsky B. M., Jenkins J. S., Ivanyuk O. M., Jones H. R. A., Lyubchik Y. P., 2019, *A&A*, 621, A112

Petigura E. A., Marcy G. W., 2011, *ApJ*, 735, 41

Quirrenbach A., et al., 2020, in Society of Photo-Optical Instrumentation Engineers (SPIE) Conference Series. p. 114473C, doi:10.1117/12.2561380

Ramírez I., Allende Prieto C., Lambert D. L., 2007, *A&A*, 465, 271

Ramírez I., Allende Prieto C., Lambert D. L., 2013, *ApJ*, 764, 78

Raskin G., et al., 2011, *A&A*, 526, A69

Reddy B. E., Lambert D. L., Allende Prieto C., 2006, *MNRAS*, 367, 1329

Reid I. N., Gizis J. E., Cohen J. G., Pahre M. A., Hogg D. W., Cowie L., Hu E., Songaila A., 1997, *PASP*, 109, 559

Reylé C., Jardine K., Fouqué P., Caballero J. A., Smart R. L., Sozzetti A., 2021, *A&A*, 650, A201

Ribas I., et al., 2023, *A&A*, 670, A139

Rojas-Ayala B., Covey K. R., Muirhead P. S., Lloyd J. P., 2010, *ApJ*, 720, L113

Rutten R. J., 1988, in Viotti R., Vittone A., Friedjung M., eds, *Astrophysics and Space Science Library* Vol. 138, IAU Colloq. 94: Physics of Formation of FE II Lines Outside LTE. pp 185–210, doi:10.1007/978-94-009-4023-9_23

Ryabchikova T., Piskunov N., Kurucz R. L., Stempels H. C., Heiter U., Pakhomov Y., Barklem P. S., 2015, *Phys. Scr.*, 90, 054005

Scalo J., et al., 2007, *Astrobiology*, 7, 85

Seager S., Deming D., 2010, *ARA&A*, 48, 631

Seitzzahl I. R., Cescutti G., Röpkke F. K., Ruitter A. J., Pakmor R., 2013, *A&A*, 559, L5

Shan Y., et al., 2021, *A&A*, 654, A118

Shields A. L., Ballard S., Johnson J. A., 2016, *Phys. Rep.*, 663, 1

Snedden C. A., 1973, PhD thesis, University of Texas, Austin

Snedden C., Cowan J. J., Kobayashi C., Pignatari M., Lawler J. E., Den Hartog E. A., Wood M. P., 2016, *ApJ*, 817, 53

Sousa S. G., Santos N. C., Adibekyan V., Delgado-Mena E., Israelian G., 2015, *A&A*, 577, A67

Souto D., et al., 2020, *ApJ*, 890, 133

Souto D., et al., 2022, *ApJ*, 927, 123

Steenbock W., Holweger H., 1984, *A&A*, 130, 319

Stonkutė E., et al., 2020, *AJ*, 159, 90

Suárez-Andrés L., Israelian G., González Hernández J. I., Adibekyan V. Z., Delgado Mena E., Santos N. C., Sousa S. G., 2018, *A&A*, 614, A84

Taberner H. M., Montes D., González Hernández J. I., 2012, *A&A*, 547, A13

Taberner H. M., Marfil E., Montes D., González Hernández J. I., 2019, *A&A*, 628, A131

Taberner H. M., et al., 2021, *A&A*, 646, A158

Takeda Y., Honda S., 2005, *PASJ*, 57, 65

Tarter J. C., et al., 2007, *Astrobiology*, 7, 30

Terrien R. C., Mahadevan S., Bender C. F., Deshpande R., Ramsey L. W., Bochanski J. J., 2012, *ApJ*, 747, L38

Thévenin F., Idiart T. P., 1999, *ApJ*, 521, 753

Thiabaud A., Marboeuf U., Alibert Y., Leya I., Mezger K., 2015, *A&A*, 580, A30

Tolstoy E., Hill V., Tosi M., 2009, *ARA&A*, 47, 371

Tsujimoto T., Shigezawa T., 1998, *ApJ*, 508, L151

Voronov Y. V., Yakovleva S. A., Belyaev A. K., 2022, *ApJ*, 926, 173

Weingartner J. C., Draine B. T., 2001, *ApJ*, 548, 296

Winters J. G., et al., 2015, *AJ*, 149, 5

Woolf V. M., Wallerstein G., 2006, *PASP*, 118, 218

Woosley S. E., Weaver T. A., 1995, *ApJS*, 101, 181

Zhao G., Chen Y. Q., Qiu H. M., Li Z. W., 2002, *AJ*, 124, 2224

Zhao G., et al., 2016, *ApJ*, 833, 225

da Silva R., Milone A. d. C., Rocha-Pinto H. J., 2015, *A&A*, 580, A24

APPENDIX A: LONG TABLES

Here we provide the tables with the abundances for the whole sample, and the HFS components for the Sc, V, Mn, and Co lines.

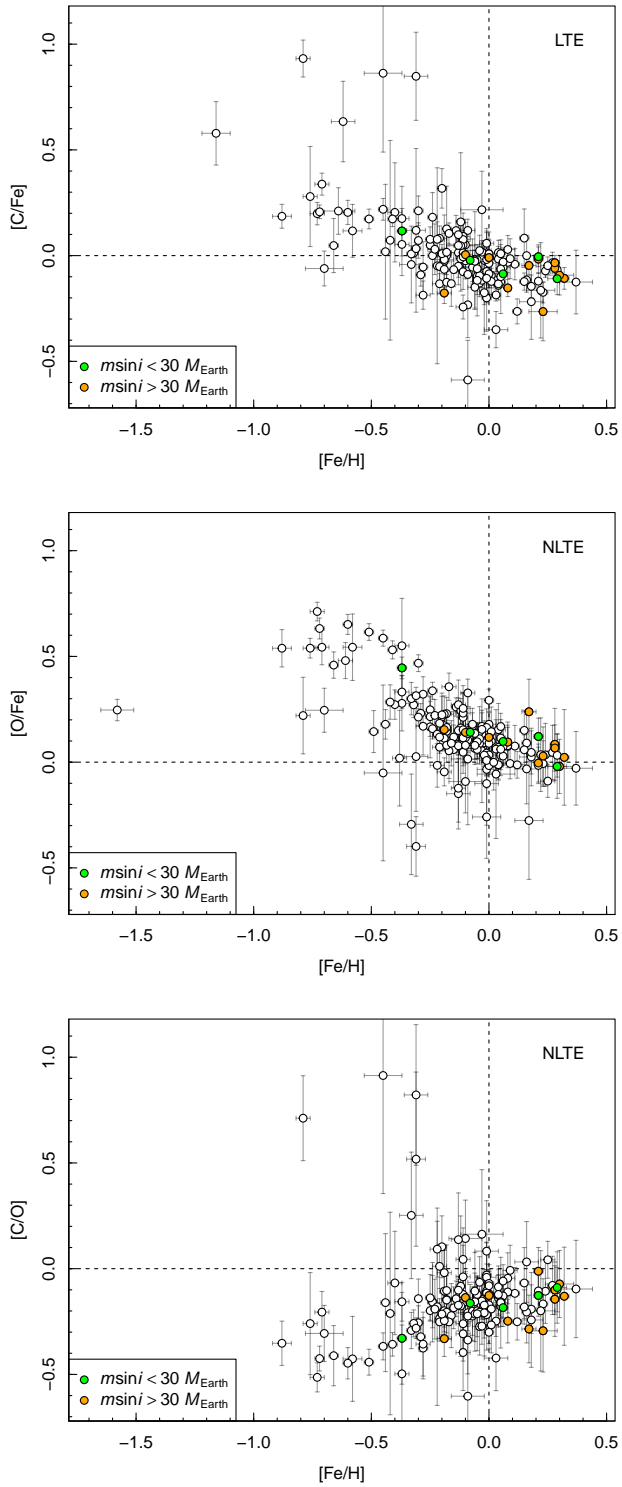


Figure 9. Abundance ratios of $[\text{C}/\text{Fe}]$, $[\text{O}/\text{Fe}]$, and $[\text{C}/\text{O}]$ versus $[\text{Fe}/\text{H}]$, indicating the stars with exoplanets, and colour-coded by $M \sin i$.

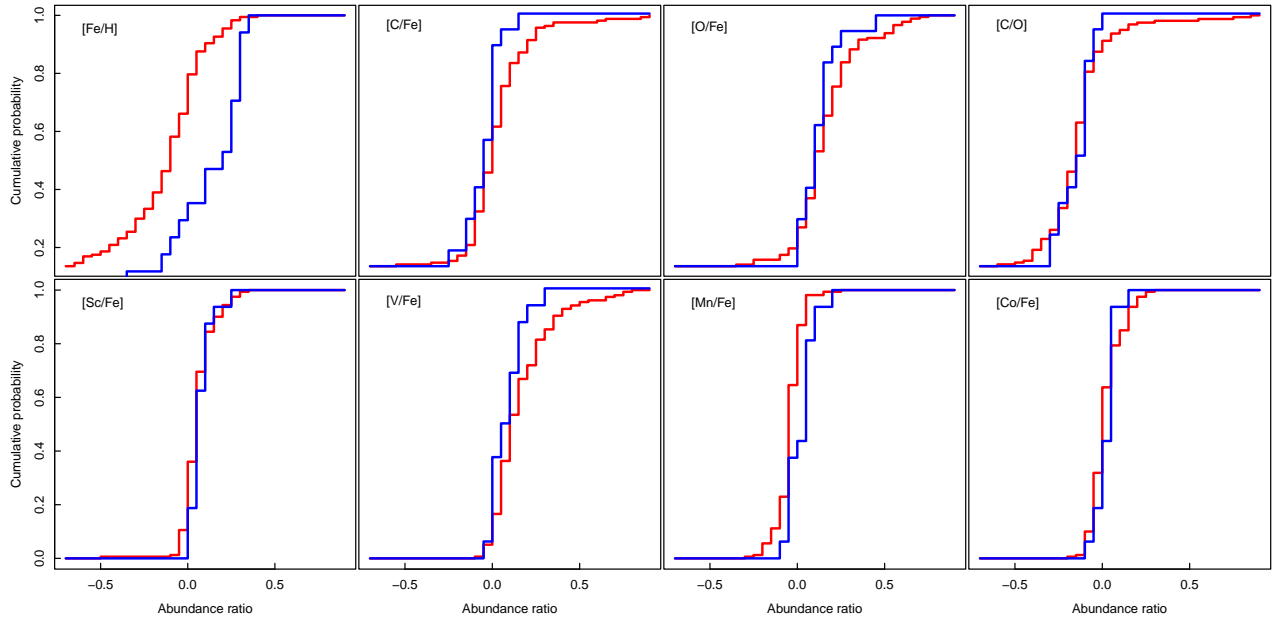


Figure 10. Normalised cumulative distribution function of the abundance ratios of several elements of the stars in our sample with (blue) and without (red) detected exoplanets.

Table A1. Abundances [X/H] with respect to the Sun for C, O, Sc, V, Mn, and Co.

WDS	Primary	RA (J2000)	DEC (J2000)	Spectral type	[C/H] (dex)	[O/H] ^{LTE} (dex)	[O/H] ^{NLTE} (dex)	[Sc/H] (dex)	[V/H] (dex)	[Mn/H] ^{LTE} (dex)	[Mn/H] ^{NLTE} (dex)	[Co/H] ^{LTE} (dex)	[Co/H] ^{NLTE} (dex)	Notes ^a
00153+5304	G 217-41	00:15:14.8	+53:04:27	K3 V	-0.32 ± 0.09	0.06 ± 0.14	0.10 ± 0.13	0.00 ± 0.07	0.13 ± 0.11	0.07 ± 0.10	0.06 ± 0.10	0.02 ± 0.09	-0.05 ± 0.11	
00385+4300	BD+42 126	00:38:29.2	+43:00:00	G5 V	-0.76 ± 0.08	-0.52 ± 0.11	-0.45 ± 0.10	-0.51 ± 0.09	-0.38 ± 0.13	-0.83 ± 0.08	-0.83 ± 0.07	-0.56 ± 0.06	-0.60 ± 0.06	
00452+0015	HD 4271 Aa,Ab	00:45:11.0	+00:15:12	F8 V	0.11 ± 0.06	0.21 ± 0.12	0.15 ± 0.10	0.10 ± 0.10	0.28 ± 0.21	0.00 ± 0.11	0.01 ± 0.11	0.01 ± 0.05	0.02 ± 0.04	
00467-0426	HD 4449	00:46:40.5	-04:25:37	G5 V	-0.05 ± 0.10	-0.23 ± 0.17	-0.19 ± 0.15	-0.09 ± 0.20	0.16 ± 0.11	0.13 ± 0.14	0.12 ± 0.14	0.04 ± 0.06	0.02 ± 0.06	
00491+5749	Achird Aa,Ab	00:49:06.2	+57:48:55	G0 V	-0.20 ± 0.02	-0.01 ± 0.05	0.00 ± 0.04	-0.24 ± 0.07	-0.30 ± 0.06	-0.36 ± 0.07	-0.35 ± 0.07	-0.30 ± 0.06	-0.26 ± 0.06	
01055+1523	HD 6440 A	01:05:29.9	+15:23:24	K3.5 V	...	-0.14 ± 0.16	-0.08 ± 0.15	-0.24 ± 0.17	-0.03 ± 0.11	-0.35 ± 0.18	-0.41 ± 0.18	-0.18 ± 0.12	-0.28 ± 0.10	
01076+2257	HD 6660 A	01:07:37.9	+22:57:19	K4 V	...	-0.17 ± 0.34	-0.03 ± 0.30	0.05 ± 0.26	0.45 ± 0.27	0.10 ± 0.13	0.05 ± 0.13	0.15 ± 0.16	0.15 ± 0.12	
01187-0052	HD 7895	01:18:41.1	-00:52:03	K0 V+	-0.18 ± 0.05	-0.09 ± 0.06	-0.04 ± 0.05	-0.16 ± 0.10	-0.04 ± 0.05	-0.18 ± 0.06	-0.20 ± 0.07	-0.16 ± 0.05	-0.20 ± 0.05	
01215+3120	EN Psc	01:21:28.2	+31:20:29	K2 V	-0.04 ± 0.06	0.04 ± 0.09	0.09 ± 0.08	-0.09 ± 0.08	0.14 ± 0.08	0.00 ± 0.05	-0.03 ± 0.05	0.01 ± 0.06	-0.06 ± 0.08	
01226+1245	BD+12 168 A	01:22:36.6	+12:45:04	K3 V	0.19 ± 0.18	-0.03 ± 0.26	0.02 ± 0.25	-0.03 ± 0.14	0.21 ± 0.21	-0.01 ± 0.11	-0.04 ± 0.11	-0.02 ± 0.14	-0.05 ± 0.11	
01230-1258	HD 8389 A	01:23:02.6	-12:57:58	K0 V	0.31 ± 0.10	0.33 ± 0.20	0.34 ± 0.17	0.40 ± 0.11	0.54 ± 0.12	0.49 ± 0.08	0.48 ± 0.08	0.46 ± 0.09	0.41 ± 0.10	
01340-0141	BD-02 247	01:34:02.1	-01:41:10	G5 V	-0.53 ± 0.05	-0.06 ± 0.05	-0.02 ± 0.04	-0.60 ± 0.11	-0.72 ± 0.15	-0.99 ± 0.19	-0.94 ± 0.18	-0.64 ± 0.12	-0.59 ± 0.09	
01450-0104	BD-01 237	01:44:59.1	-01:03:31	K0 V	-0.32 ± 0.05	0.13 ± 0.28	0.18 ± 0.22	-0.30 ± 0.12	-0.25 ± 0.08	-0.46 ± 0.05	-0.47 ± 0.04	-0.34 ± 0.04	-0.37 ± 0.04	
01572-1015	HD 11964 A	01:57:09.6	-10:14:33	G8 IV	-0.03 ± 0.05	0.17 ± 0.09	0.16 ± 0.07	0.03 ± 0.06	0.07 ± 0.06	0.01 ± 0.04	0.00 ± 0.04	0.00 ± 0.08	0.00 ± 0.07	
02290-1959	HD 15468	02:29:01.7	-19:58:45	K4 V+	-0.19 ± 0.39	-0.77 ± 0.14	-0.71 ± 0.14	-0.33 ± 0.33	0.20 ± 0.14	-0.45 ± 0.16	-0.52 ± 0.13	-0.30 ± 0.14	-0.32 ± 0.15	
02291+2252	BD+22 353 Aa,Ab	02:29:07.3	+22:52:05	K0 V	-0.12 ± 0.08	0.06 ± 0.09	0.10 ± 0.08	-0.01 ± 0.09	0.15 ± 0.09	-0.11 ± 0.07	-0.12 ± 0.07	0.01 ± 0.06	-0.04 ± 0.05	
02361+0653	HD 16160 A	02:36:04.9	+06:53:13	K0 V+	0.12 ± 0.09	-0.04 ± 0.11	0.01 ± 0.11	-0.11 ± 0.16	0.15 ± 0.10	-0.24 ± 0.06	-0.28 ± 0.06	-0.11 ± 0.10	-0.16 ± 0.09	
02442+4914	θ Per A	02:44:12.0	+49:13:42	F7 V	0.05 ± 0.06	0.25 ± 0.14	0.19 ± 0.12	0.02 ± 0.08	0.26 ± 0.33	-0.02 ± 0.10	0.00 ± 0.12	-0.05 ± 0.08	-0.02 ± 0.08	
02482+2704	BC Ari Aa,Ab	02:48:09.1	+27:04:07	K1 V	-0.04 ± 0.15	0.11 ± 0.11	0.14 ± 0.09	-0.09 ± 0.10	0.09 ± 0.06	0.00 ± 0.06	-0.02 ± 0.07	-0.05 ± 0.06	-0.10 ± 0.08	
02556+2652	HD 18143 A	02:55:39.1	+26:52:24	K2 IV	-0.04 ± 0.18	0.17 ± 0.15	0.20 ± 0.14	0.19 ± 0.09	0.33 ± 0.10	0.18 ± 0.07	0.15 ± 0.07	0.20 ± 0.08	0.16 ± 0.10	
03042+6142	HD 18757	03:04:09.6	+61:42:21	G4 V	-0.09 ± 0.07	0.14 ± 0.05	0.17 ± 0.04	-0.11 ± 0.08	-0.19 ± 0.06	-0.41 ± 0.16	-0.45 ± 0.11	-0.20 ± 0.04	-0.19 ± 0.02	
03078+2533	HD 19381 A	03:07:50.5	+25:33:07	F8 V	0.07 ± 0.07	0.23 ± 0.11	0.19 ± 0.10	0.13 ± 0.11	0.05 ± 0.13	0.07 ± 0.06	0.09 ± 0.06	-0.01 ± 0.07	0.00 ± 0.09	
03150+0101	BD+00 549 A	03:15:04.8	+01:02:15	G5 V	-0.69 ± 0.06	-0.40 ± 0.11	-0.34 ± 0.09	-0.65 ± 0.12	-0.68 ± 0.21	-1.19 ± 0.27	-1.20 ± 0.27	-0.67 ± 0.10	-0.64 ± 0.12	
03206+0902	HD 20727 Aa,Ab	03:20:37.0	+09:02:01	G0 V	-0.06 ± 0.12	0.07 ± 0.05	0.10 ± 0.04	-0.01 ± 0.07	-0.10 ± 0.09	-0.39 ± 0.07	-0.37 ± 0.07	-0.10 ± 0.06	-0.09 ± 0.06	
03321+4340	HD 21727 A	03:32:05.1	+43:40:12	G5 V	-0.04 ± 0.08	0.09 ± 0.06	0.10 ± 0.05	0.02 ± 0.06	0.00 ± 0.07	-0.10 ± 0.05	-0.10 ± 0.06	-0.02 ± 0.09	-0.07 ± 0.03	
03332+4615	V577 Per	03:33:13.5	+46:15:27	G5 V	0.03 ± 0.05	0.20 ± 0.07	0.24 ± 0.07	-0.08 ± 0.10	0.12 ± 0.07	-0.07 ± 0.13	-0.09 ± 0.15	-0.13 ± 0.12	-0.18 ± 0.12	
03356+4253	HD 22122	03:35:35.8	+42:53:15	F8 V	-0.19 ± 0.05	-0.02 ± 0.09	-0.04 ± 0.08	-0.29 ± 0.10	-0.31 ± 0.22	-0.42 ± 0.11	-0.36 ± 0.12	-0.34 ± 0.08	-0.22 ± 0.11	
03396+1823	V1082 Tau Aa,Ab	03:39:33.6	+18:23:06	G5+	SB2
03398+3328	HD 278874 Aa,Ab	03:39:49.0	+33:28:24	K2	SB2
03480+4032	HD 23596	03:48:00.4	+40:31:50	F8 V	0.22 ± 0.04	0.45 ± 0.20	0.36 ± 0.17	0.34 ± 0.09	0.26 ± 0.10	0.27 ± 0.06	0.28 ± 0.07	0.28 ± 0.07	0.29 ± 0.09	
03520+3947	HD 275867	03:52:00.3	+39:47:44	K2 V	...	-0.34 ± 0.17	-0.28 ± 0.17	-0.16 ± 0.21	0.19 ± 0.16	-0.15 ± 0.10	-0.19 ± 0.09	-0.15 ± 0.09	-0.20 ± 0.10	
03556+5214	HD 24421	03:55:37.1	+52:13:37	F8 V	-0.31 ± 0.02	-0.04 ± 0.07	-0.05 ± 0.06	-0.23 ± 0.08	-0.30 ± 0.08	-0.43 ± 0.12	-0.40 ± 0.13	-0.33 ± 0.05	-0.23 ± 0.08	
03566+5042	43 Per Aa,Ab	03:56:36.5	+50:41:43	F5 V	SB2
03575-0110	HD 24916 A	03:57:28.7	-01:09:34	K4 V	...	-0.10 ± 0.21	-0.04 ± 0.19	-0.13 ± 0.20	0.20 ± 0.16	-0.25 ± 0.20	-0.32 ± 0.18	-0.08 ± 0.13	-0.12 ± 0.13	
04153-0739	o ² Eri A	04:15:16.3	-07:39:10	K0.5 V	-0.25 ± 0.21	0.02 ± 0.06	0.08 ± 0.05	-0.17 ± 0.08	-0.08 ± 0.06	-0.45 ± 0.05	-0.47 ± 0.05	-0.20 ± 0.05	-0.24 ± 0.05	
04252+2545	HD 27887 A	04:25:10.8	+25:44:57	F5	Hot
04359+1631	Aldebaran	04:35:55.2	+16:30:33	K5 III	Cool
04397+0952	HD 286955	04:39:42.6	+09:52:19	K2 V+	...	-0.15 ± 0.13	-0.09 ± 0.13	-0.23 ± 0.22	0.03 ± 0.12	-0.38 ± 0.09	-0.42 ± 0.09	-0.24 ± 0.08	-0.28 ± 0.09	
04429+1843	HD 29836	04:42:51.7	+18:43:14	G2 V	0.17 ± 0.03	0.32 ± 0.18	0.27 ± 0.15	0.33 ± 0.04	0.25 ± 0.06	0.16 ± 0.06	0.16 ± 0.07	0.29 ± 0.05	0.27 ± 0.03	
04559+0440	HD 31412	04:55:55.9	+04:40:14	F9.5 V+	0.05 ± 0.05	0.20 ± 0.10	0.16 ± 0.09	0.11 ± 0.08	0.15 ± 0.11	0.06 ± 0.08	0.08 ± 0.08	0.03 ± 0.04	0.06 ± 0.05	
05003+2508	HD 31867 A	05:00:17.5	+25:08:11	G2 V	0.00 ± 0.12	0.02 ± 0.12	0.03 ± 0.10	0.02 ± 0.08	-0.01 ± 0.07	-0.07 ± 0.11	-0.07 ± 0.12	-0.03 ± 0.05	-0.04 ± 0.04	
05067+5136	9 Aur Aa,Ab	05:06:40.6	+51:35:52	F2 V+M2	Hot
05189-2124	HD 34751 A	05:18:47.2	-21:23:38	K6 V	0.54 ± 0.21	-0.35 ± 0.28	-0.28 ± 0.26	-0.03 ± 0.38	0.31 ± 0.23	-0.34 ± 0.29	-0.44 ± 0.27	0.00 ± 0.19	-0.04 ± 0.16	
05264+0351	HD 35638	05:26:23.1	+03:51:24	F5 V	0.01 ± 0.07	0.24 ± 0.13	0.18 ± 0.12	0.03 ± 0.08	0.34 ± 0.36	-0.10 ± 0.08	-0.07 ± 0.09	-0.04 ± 0.08	0.03 ± 0.08	
05289+1233	HD 35956 Aa,Ab	05:28:51.6	+12:33:03	G0 V	-0.07 ± 0.05	0.07 ± 0.08	0.06 ± 0.07	-0.02 ± 0.08	-0.02 ± 0.14	-0.14 ± 0.07	-0.13 ± 0.08	-0.15 ± 0.06	-0.12 ± 0.04	
05413+5329	V538 Aur	05:41:20.3	+53:28:52	K1 V	-0.10 ± 0.07	-0.01 ± 0.08	0.03 ± 0.07	-0.02 ± 0.09	0.14 ± 0.05	0.02 ± 0.04	-0.01 ± 0.04	-0.04 ± 0.05	-0.07 ± 0.06	
05427+0241	HD 38014	05:42:45.8	+02:40:45	K1 V	-0.17 ± 0.06	0.06 ± 0.14	0.10 ± 0.12	-0.03 ± 0.11	0.16 ± 0.09	-0.04 ± 0.15	-0.06 ± 0.16	0.00 ± 0.06	-0.05 ± 0.07	
05445-2227	γ Lep	05:44:27.8	-22:26:54	F6 V	-0.01 ± 0.06	0.16 ± 0.11	0.12 ± 0.09	0.01 ± 0.13	0.17 ± 0.20	-0.14 ± 0.06	-0.12 ± 0.06	-0.11 ± 0.08	-0.05 ± 0.11	
	AK Lep	05:44:26.5	-22:25:19	K2 V	0.03 ± 0.08	-0.15 ± 0.12	-0.10 ± 0.11	-0.15 ± 0.12	0.08 ± 0.10	-0.20 ± 0.11	-0.24 ± 0.11	-0.14 ± 0.07	-0.20 ± 0.08	

Table A1 – continued

WDS	Primary	RA (J2000)	DEC (J2000)	Spectral type	[C/H] (dex)	[O/H] ^{LTE} (dex)	[O/H] ^{NLTE} (dex)	[Sc/H] (dex)	[V/H] (dex)	[Mn/H] ^{LTE} (dex)	[Mn/H] ^{NLTE} (dex)	[Co/H] ^{LTE} (dex)	[Co/H] ^{NLTE} (dex)	Notes ^a
05466+0110	HD 38529 A	05:46:34.9	+01:10:05	G4 IV	0.21 ± 0.05	0.44 ± 0.27	0.34 ± 0.23	0.32 ± 0.08	0.32 ± 0.07	0.37 ± 0.08	0.38 ± 0.09	0.31 ± 0.05	0.31 ± 0.05	
05584-0439	HD 40397 A	05:58:21.5	-04:39:02	G7 V	-0.02 ± 0.07	0.09 ± 0.05	0.12 ± 0.04	0.00 ± 0.09	-0.09 ± 0.05	-0.19 ± 0.09	-0.19 ± 0.09	-0.10 ± 0.03	-0.11 ± 0.03	
06066+0431	Ross 413	06:06:30.0	+04:30:41	K4 V	-0.46 ± 0.13	-0.11 ± 0.17	-0.04 ± 0.16	-0.32 ± 0.33	0.10 ± 0.16	-0.57 ± 0.08	-0.62 ± 0.07	-0.30 ± 0.06	-0.38 ± 0.05	
06173+0506	HD 43587	06:17:16.1	+05:06:00	F9 V	-0.01 ± 0.02	0.16 ± 0.09	0.14 ± 0.08	-0.02 ± 0.08	-0.04 ± 0.07	-0.05 ± 0.09	-0.04 ± 0.10	-0.09 ± 0.04	-0.06 ± 0.04	
06314-0134	HD 291763	06:31:23.1	-01:34:14	K2 V	...	-0.19 ± 0.09	-0.13 ± 0.09	-0.43 ± 0.10	-0.26 ± 0.08	-0.79 ± 0.15	-0.83 ± 0.16	-0.47 ± 0.06	-0.51 ± 0.06	
06319+0039	HD 291725	06:31:51.4	+00:38:59	G7 V	-0.38 ± 0.05	-0.09 ± 0.05	-0.06 ± 0.05	-0.19 ± 0.05	-0.22 ± 0.07	-0.47 ± 0.07	-0.46 ± 0.08	-0.29 ± 0.09	-0.32 ± 0.08	
06332+0528	HD 46375 A	06:33:12.6	+05:27:47	K1 V	-0.03 ± 0.14	0.23 ± 0.16	0.26 ± 0.14	0.27 ± 0.06	0.35 ± 0.10	0.25 ± 0.13	0.22 ± 0.14	0.29 ± 0.07	0.24 ± 0.09	
06368+3751	BD+37 1545	06:36:46.4	+37:51:07	G5 V	0.00 ± 0.05	0.11 ± 0.11	0.13 ± 0.09	0.08 ± 0.05	0.09 ± 0.07	0.11 ± 0.10	0.10 ± 0.11	0.08 ± 0.05	0.05 ± 0.06	
06461+3233	HD 263175 A	06:46:05.1	+32:33:20	K3 V	...	-0.42 ± 0.26	-0.36 ± 0.23	-0.38 ± 0.10	-0.20 ± 0.10	-0.43 ± 0.06	-0.47 ± 0.05	-0.36 ± 0.07	-0.41 ± 0.08	
06523-0510	HD 50281 A	06:52:18.1	-05:10:25	K3.5 V	...	-0.15 ± 0.19	-0.09 ± 0.18	-0.18 ± 0.22	0.17 ± 0.16	-0.16 ± 0.11	-0.21 ± 0.11	-0.14 ± 0.10	-0.18 ± 0.08	
07041+7514	HD 51067 A	07:04:03.9	+75:13:39	G0 V	0.03 ± 0.05	0.27 ± 0.12	0.23 ± 0.10	0.17 ± 0.07	0.18 ± 0.09	0.13 ± 0.07	0.14 ± 0.08	0.07 ± 0.04	0.07 ± 0.04	
	HD 51067 B	07:04:05.7	+75:13:50	G5	-0.08 ± 0.06	0.08 ± 0.06	0.11 ± 0.05	0.05 ± 0.07	0.15 ± 0.05	0.05 ± 0.07	0.02 ± 0.07	0.04 ± 0.06	0.03 ± 0.05	
07058+8337	HD 48974	07:05:49.9	+83:36:44	G5 V	-0.22 ± 0.08	-0.06 ± 0.07	-0.03 ± 0.06	-0.16 ± 0.10	-0.15 ± 0.07	-0.21 ± 0.05	-0.21 ± 0.05	-0.16 ± 0.06	-0.19 ± 0.05	
07191+6644	HD 55745 A	07:19:08.3	+66:44:23	F8 V	0.06 ± 0.05	0.28 ± 0.13	0.22 ± 0.11	0.21 ± 0.12	0.23 ± 0.11	0.21 ± 0.07	0.23 ± 0.07	0.11 ± 0.07	0.14 ± 0.07	
07321-0853	HD 59984	07:32:05.8	-08:52:53	G0 V	-0.61 ± 0.13	-0.22 ± 0.07	-0.20 ± 0.06	-0.50 ± 0.10	-0.62 ± 0.06	-0.81 ± 0.18	-0.74 ± 0.20	-0.67 ± 0.12	-0.50 ± 0.15	
07400-0336	V869 Mon	07:39:59.3	-03:35:51	K2 V	-0.02 ± 0.11	-0.12 ± 0.10	-0.06 ± 0.10	-0.17 ± 0.10	0.03 ± 0.04	-0.16 ± 0.06	-0.18 ± 0.06	-0.13 ± 0.07	-0.21 ± 0.06	
08082+7155	HD 66171	08:08:10.5	+71:55:28	G2 V	-0.33 ± 0.12	0.02 ± 0.10	0.04 ± 0.08	-0.23 ± 0.09	-0.34 ± 0.09	-0.40 ± 0.09	-0.39 ± 0.10	-0.28 ± 0.11	-0.28 ± 0.05	
08082+2106	BD+21 1764 A	08:08:13.2	+21:06:18	K7 V	0.41 ± 0.37	-0.55 ± 0.42	-0.50 ± 0.42	-0.15 ± 0.43	0.29 ± 0.38	-0.47 ± 0.24	-0.55 ± 0.21	-0.31 ± 0.21	-0.33 ± 0.18	
08107-1348	18 Pup A	08:10:39.8	-13:47:57	F6.5 V	0.05 ± 0.05	0.19 ± 0.10	0.15 ± 0.09	0.06 ± 0.08	-0.02 ± 0.11	-0.03 ± 0.11	-0.01 ± 0.12	-0.01 ± 0.10	0.01 ± 0.06	
08110+7955	BD+80 245	08:11:06.2	+79:54:30	G0 IV	...	-1.39 ± 0.08	-1.33 ± 0.05	-2.09 ± 0.17	...	-1.91 ± 0.30	-1.82 ± 0.28	
08138+6306	HD 67850	08:13:45.8	+63:06:14	G0 V	-0.32 ± 0.16	-0.01 ± 0.05	0.01 ± 0.04	-0.08 ± 0.06	-0.11 ± 0.04	-0.18 ± 0.05	-0.19 ± 0.05	-0.17 ± 0.06	-0.14 ± 0.05	
08161+5706	HD 68638	08:16:06.3	+57:05:39	G8 V	-0.24 ± 0.18	-0.13 ± 0.06	-0.08 ± 0.05	-0.24 ± 0.07	-0.21 ± 0.04	-0.30 ± 0.06	-0.31 ± 0.07	-0.30 ± 0.06	-0.32 ± 0.04	
08484+2042	HD 75076	08:48:24.0	+20:41:47	F8 V	-0.15 ± 0.03	0.16 ± 0.09	0.13 ± 0.08	0.01 ± 0.11	0.04 ± 0.15	-0.16 ± 0.11	-0.14 ± 0.12	-0.10 ± 0.06	-0.06 ± 0.04	
08492+0329	HD 75302	08:49:12.5	+03:29:05	G5 V	-0.07 ± 0.03	0.07 ± 0.08	0.08 ± 0.07	0.04 ± 0.07	0.03 ± 0.05	-0.03 ± 0.07	-0.05 ± 0.07	-0.01 ± 0.05	-0.02 ± 0.05	
08526+2820	ρ^{01} Cnc A	08:52:35.8	+28:19:51	G8 V	0.18 ± 0.08	0.25 ± 0.18	0.27 ± 0.15	0.34 ± 0.08	0.43 ± 0.09	0.36 ± 0.06	0.34 ± 0.07	0.36 ± 0.07	0.32 ± 0.08	
09008+2347	HD 77052	09:00:49.3	+23:46:48	G2 V	0.02 ± 0.06	0.11 ± 0.09	0.11 ± 0.08	0.05 ± 0.06	0.04 ± 0.10	0.00 ± 0.06	0.00 ± 0.07	0.02 ± 0.03	0.02 ± 0.04	
09029+0600	BD+06 2091	09:02:51.3	+06:00:28	G0 V	0.04 ± 0.33	0.10 ± 0.07	0.12 ± 0.06	-0.07 ± 0.13	0.02 ± 0.15	-0.17 ± 0.11	-0.17 ± 0.13	-0.08 ± 0.06	-0.09 ± 0.05	
09058+5532	HD 77599	09:05:45.9	+55:31:44	G0 V	-0.16 ± 0.03	0.11 ± 0.08	0.09 ± 0.07	0.01 ± 0.08	0.01 ± 0.10	-0.04 ± 0.09	-0.03 ± 0.10	-0.06 ± 0.06	-0.02 ± 0.05	
09152+2323	HD 79498	09:15:09.4	+23:22:32	G5 V	0.19 ± 0.07	0.23 ± 0.11	0.21 ± 0.09	0.25 ± 0.07	0.21 ± 0.07	0.27 ± 0.10	0.27 ± 0.11	0.21 ± 0.04	0.19 ± 0.05	
09211+6024	BD+61 1116	09:21:06.8	+60:24:11	K0 V	-0.27 ± 0.46	-0.13 ± 0.06	-0.09 ± 0.05	-0.20 ± 0.10	-0.07 ± 0.07	-0.24 ± 0.06	-0.26 ± 0.06	-0.19 ± 0.07	-0.24 ± 0.08	
09245+0621	HD 81212 AB	09:24:28.6	+06:21:00	F5	SB2
09327+2659	DX Leo	09:32:43.8	+26:59:19	G9 V	-0.06 ± 0.12	0.06 ± 0.05	0.10 ± 0.04	-0.15 ± 0.07	-0.02 ± 0.06	-0.10 ± 0.07	-0.11 ± 0.07	-0.19 ± 0.08	-0.26 ± 0.07	
09353-1019	HD 83008	09:35:17.9	-10:18:51	K0 V	-0.12 ± 0.15	-0.30 ± 0.20	-0.25 ± 0.16	-0.16 ± 0.12	0.05 ± 0.06	-0.14 ± 0.16	-0.16 ± 0.17	-0.12 ± 0.07	-0.15 ± 0.05	
09361+3733	HD 82939	09:36:04.3	+37:33:10	G5 V	0.03 ± 0.07	0.07 ± 0.05	0.09 ± 0.04	0.00 ± 0.07	0.09 ± 0.05	0.05 ± 0.04	0.04 ± 0.04	0.02 ± 0.03	-0.02 ± 0.04	
09393+1319	HD 83509 Aa,Ab	09:39:17.2	+13:18:45	F7 V	SB2
10010+3155	20 LMi A	10:01:00.7	+31:55:25	G3 V	0.09 ± 0.04	0.22 ± 0.10	0.19 ± 0.09	0.25 ± 0.05	0.20 ± 0.05	0.20 ± 0.05	0.20 ± 0.05	0.21 ± 0.04	0.20 ± 0.04	
10172+2306	39 Leo A	10:17:14.6	+23:06:23	F8 V	-0.32 ± 0.04	-0.02 ± 0.09	-0.03 ± 0.08	-0.26 ± 0.13	-0.27 ± 0.33	-0.45 ± 0.13	-0.42 ± 0.14	0.34 ± 0.13	-0.32 ± 0.08	
10306+5559	36 UMa A	10:30:37.6	+55:58:50	F8 V	-0.15 ± 0.02	0.08 ± 0.10	0.05 ± 0.08	-0.07 ± 0.08	0.03 ± 0.12	-0.17 ± 0.08	-0.16 ± 0.08	-0.20 ± 0.08	-0.16 ± 0.05	
10504-1326	BD-12 3277	10:50:22.4	-13:26:07	G3 V	-0.12 ± 0.09	0.00 ± 0.09	0.02 ± 0.09	-0.06 ± 0.05	-0.12 ± 0.07	-0.23 ± 0.09	-0.23 ± 0.10	-0.12 ± 0.05	-0.12 ± 0.04	
10507+5148	LZ UMa	10:50:40.3	+51:47:59	G5 V	-0.10 ± 0.05	-0.03 ± 0.07	0.03 ± 0.07	-0.10 ± 0.08	0.04 ± 0.08	-0.11 ± 0.05	-0.15 ± 0.05	-0.13 ± 0.10	-0.23 ± 0.06	
11047-0413	HH Leo	11:04:41.5	-04:13:16	G8 V	-0.10 ± 0.15	0.04 ± 0.04	0.07 ± 0.04	-0.07 ± 0.08	0.02 ± 0.08	-0.01 ± 0.06	-0.01 ± 0.06	-0.14 ± 0.05	-0.16 ± 0.04	
11152+7329	HD 97584 A	11:15:11.9	+73:28:31	K4 V	...	-0.18 ± 0.13	-0.12 ± 0.13	-0.14 ± 0.13	0.13 ± 0.12	-0.21 ± 0.09	-0.25 ± 0.09	-0.15 ± 0.08	-0.21 ± 0.08	
11214-2027	SZ Cr1	11:21:26.6	-20:27:13	K7 V	Cool
11218+1811	HD 98736	11:21:49.3	+18:11:24	K0 V	0.21 ± 0.09	0.26 ± 0.14	0.28 ± 0.13	0.32 ± 0.10	0.41 ± 0.10	0.47 ± 0.17	0.47 ± 0.16	0.38 ± 0.07	0.33 ± 0.08	
11378+4150	BD+42 2230 A	11:37:50.8	+41:49:32	G6 V	-0.19 ± 0.08	0.09 ± 0.12	0.12 ± 0.10	-0.11 ± 0.07	-0.07 ± 0.07	-0.17 ± 0.07	-0.17 ± 0.08	-0.08 ± 0.10	-0.15 ± 0.04	
11403+0931	BD+10 2321	11:40:16.6	+09:30:44	K0 V	-0.47 ± 0.07	-0.17 ± 0.16	-0.11 ± 0.14	-0.36 ± 0.08	-0.25 ± 0.09	-0.37 ± 0.12	-0.41 ± 0.13	-0.35 ± 0.05	-0.43 ± 0.05	
11455+4740	HD 102158	11:45:30.5	+47:40:01	G2 V	-0.23 ± 0.05	0.10 ± 0.05	0.14 ± 0.04	-0.29 ± 0.11	-0.32 ± 0.13	-0.65 ± 0.11	-0.63 ± 0.12	-0.38 ± 0.06	-0.35 ± 0.05	
11475+7702	HD 102326	11:47:30.3	+77:02:24	G8 IV	0.23 ± 0.14	0.29 ± 0.11	0.30 ± 0.10	0.22 ± 0.07	0.18 ± 0.06	0.15 ± 0.03	0.14 ± 0.03	0.18 ± 0.05	0.14 ± 0.06	
11523+0957	HD 103112	11:52:20.9	+09:56:53	K0 IV	0.06 ± 0.23	0.25 ± 0.19	0.26 ± 0.17	0.22 ± 0.16	0.45 ± 0.12	0.21 ± 0.18	0.26 ± 0.11	0.29 ± 0.08	0.24 ± 0.08	

Table A1 – *continued*

WDS	Primary	RA (J2000)	DEC (J2000)	Spectral type	[C/H] (dex)	[O/H] ^{LTE} (dex)	[O/H] ^{NLTE} (dex)	[Sc/H] (dex)	[V/H] (dex)	[Mn/H] ^{LTE} (dex)	[Mn/H] ^{NLTE} (dex)	[Co/H] ^{LTE} (dex)	[Co/H] ^{NLTE} (dex)	Notes ^a
12049+1729	HD 104923	12:04:57.0	+17:28:36	K0 V	-0.18 ± 0.11	-0.08 ± 0.06	-0.03 ± 0.05	-0.20 ± 0.06	-0.12 ± 0.06	-0.22 ± 0.10	-0.23 ± 0.11	-0.23 ± 0.06	-0.26 ± 0.06	
12051+1933	BD+20 2678 A	12:05:07.0	+19:33:16	G5 V	-0.09 ± 0.10	0.09 ± 0.06	0.11 ± 0.05	-0.13 ± 0.07	-0.10 ± 0.08	-0.15 ± 0.05	-0.15 ± 0.05	-0.14 ± 0.07	-0.13 ± 0.08	
12069+0548	HD 105219	12:06:56.5	+05:48:12	K0 V	-0.18 ± 0.19	-0.11 ± 0.06	-0.08 ± 0.05	-0.17 ± 0.04	-0.13 ± 0.05	-0.25 ± 0.06	-0.26 ± 0.07	-0.20 ± 0.05	-0.21 ± 0.06	
12089+2147	BD+22 2442	12:08:54.7	+21:47:19	G2 V+	-0.37 ± 0.05	-0.22 ± 0.10	-0.17 ± 0.08	-0.56 ± 0.13	-0.31 ± 0.10	-0.97 ± 0.11	-0.98 ± 0.12	-0.71 ± 0.10	-0.66 ± 0.13	
12372+3545	BD+36 2288	12:37:13.7	+35:44:46	G5 V	-0.15 ± 0.09	0.05 ± 0.10	0.05 ± 0.09	-0.06 ± 0.09	-0.02 ± 0.13	-0.09 ± 0.10	-0.08 ± 0.11	-0.11 ± 0.07	-0.14 ± 0.07	
12406+4017	HD 110279	12:40:37.4	+40:17:17	F8 V	-0.09 ± 0.07	0.03 ± 0.10	0.03 ± 0.08	0.05 ± 0.06	0.11 ± 0.08	-0.13 ± 0.17	-0.13 ± 0.19	-0.07 ± 0.06	-0.06 ± 0.06	
12482-2448	HD 111261 A	12:48:10.7	-24:48:24	K4 V	-0.32 ± 0.36	0.13 ± 0.16	-0.46 ± 0.15	-0.50 ± 0.16	-0.33 ± 0.14	-0.35 ± 0.13	
12489+1206	HD 111398	12:48:52.4	+12:05:47	G5 V	0.06 ± 0.04	0.24 ± 0.07	0.22 ± 0.06	0.10 ± 0.06	0.05 ± 0.06	0.00 ± 0.13	0.00 ± 0.14	0.05 ± 0.02	0.05 ± 0.03	
12549-0620	BD-05 3596	12:54:56.0	-06:20:19	K5 V	-0.37 ± 0.18	-0.70 ± 0.26	-0.62 ± 0.24	-0.20 ± 0.24	0.16 ± 0.20	-0.32 ± 0.14	-0.38 ± 0.13	-0.18 ± 0.12	-0.23 ± 0.13	
13018+6337	HD 113337 A	13:01:46.9	+63:36:37	F5 V	0.12 ± 0.04	0.54 ± 0.18	0.41 ± 0.15	0.21 ± 0.11	0.15 ± 0.42	0.16 ± 0.19	0.20 ± 0.21	0.05 ± 0.13	0.06 ± 0.16	
13077-1411	HD 114001	13:07:39.2	-14:11:17	F5 V	Fast
13114+0938	HD 114606 A	13:11:21.4	+09:37:34	G1 V	-0.34 ± 0.05	0.07 ± 0.04	0.11 ± 0.04	-0.33 ± 0.07	-0.37 ± 0.09	-0.69 ± 0.10	-0.67 ± 0.11	-0.48 ± 0.09	-0.39 ± 0.03	
13169+1701	HD 115404 A	13:16:51.0	+17:01:02	K2 V	-0.17 ± 0.06	-0.09 ± 0.11	-0.04 ± 0.09	-0.27 ± 0.06	-0.17 ± 0.08	-0.35 ± 0.10	-0.39 ± 0.10	-0.29 ± 0.07	-0.34 ± 0.06	
13253+4242	BD+43 2328	13:25:17.4	+42:41:58	K1 V	-0.20 ± 0.23	-0.18 ± 0.09	-0.13 ± 0.07	-0.36 ± 0.06	-0.31 ± 0.09	-0.43 ± 0.08	-0.45 ± 0.09	-0.36 ± 0.04	-0.37 ± 0.04	
13274-2138	HD 116963	13:27:24.9	-21:39:19	K4 V	-0.68 ± 0.19	-0.13 ± 0.35	-0.08 ± 0.31	-0.09 ± 0.21	0.26 ± 0.22	-0.10 ± 0.14	-0.14 ± 0.14	-0.11 ± 0.14	-0.14 ± 0.11	
13315-0800	HD 117579 A	13:31:28.7	-08:00:26	G5 V	-0.05 ± 0.20	0.02 ± 0.10	0.05 ± 0.08	-0.17 ± 0.08	-0.17 ± 0.06	-0.28 ± 0.08	-0.29 ± 0.08	-0.21 ± 0.04	-0.23 ± 0.03	
13316+5857	HD 117845	13:31:33.8	+58:57:10	G2 V	-0.22 ± 0.06	-0.02 ± 0.05	-0.02 ± 0.05	-0.15 ± 0.11	-0.09 ± 0.13	-0.29 ± 0.11	-0.27 ± 0.12	-0.27 ± 0.08	-0.22 ± 0.09	
13321-1115	HD 117676	13:32:04.7	-11:15:23	G8 V+	-0.26 ± 0.08	-0.06 ± 0.06	-0.03 ± 0.05	-0.18 ± 0.08	-0.20 ± 0.10	-0.28 ± 0.02	-0.29 ± 0.02	-0.21 ± 0.03	-0.23 ± 0.03	
13470+0621	HD 120066	13:46:57.1	+06:21:01	G0 V	-0.07 ± 0.04	0.21 ± 0.11	0.17 ± 0.09	0.23 ± 0.07	0.15 ± 0.08	-0.06 ± 0.05	-0.04 ± 0.06	0.08 ± 0.03	0.09 ± 0.02	
14050+0157	HD 122972	14:04:58.7	+01:56:59	G6 V	-0.12 ± 0.03	-0.02 ± 0.06	0.00 ± 0.05	-0.05 ± 0.09	-0.05 ± 0.05	-0.05 ± 0.05	-0.07 ± 0.03	-0.05 ± 0.04	-0.07 ± 0.05	
14196-0509	HD 125455 A	14:19:34.9	-05:09:04	K1 V	-0.34 ± 0.05	-0.14 ± 0.09	-0.09 ± 0.08	-0.16 ± 0.06	-0.05 ± 0.07	-0.22 ± 0.06	-0.24 ± 0.06	-0.17 ± 0.06	-0.20 ± 0.05	
14245+6015	BD+60 1536	14:24:26.9	+60:15:25	K5 V	-0.03 ± 0.13	-0.16 ± 0.21	-0.11 ± 0.20	-0.09 ± 0.17	0.22 ± 0.14	-0.05 ± 0.11	-0.10 ± 0.10	-0.01 ± 0.12	-0.03 ± 0.12	
14252+5151	θ Boo A	14:25:11.8	+51:51:03	F7 V	Fast
14255+2035	HD 126512	14:25:30.1	+20:35:25	F9 V	-0.40 ± 0.06	0.02 ± 0.06	0.05 ± 0.05	-0.39 ± 0.14	-0.52 ± 0.08	-0.85 ± 0.10	-0.82 ± 0.11	-0.51 ± 0.08	-0.42 ± 0.08	
14260+3422	BD+35 2558	14:25:59.9	+34:22:15	K0 V	0.14 ± 0.09	-0.63 ± 0.20	-0.57 ± 0.18	-0.62 ± 0.16	-0.46 ± 0.10	-0.96 ± 0.15	-0.97 ± 0.16	-0.72 ± 0.07	-0.76 ± 0.08	
14336+0920	HD 127871 A	14:33:34.9	+09:20:04	K2 V	-0.03 ± 0.09	-0.05 ± 0.13	0.00 ± 0.12	-0.14 ± 0.07	0.03 ± 0.08	-0.15 ± 0.08	-0.18 ± 0.08	-0.11 ± 0.09	-0.18 ± 0.11	
14415+1336	HD 129290 A	14:41:28.7	+13:36:05	G2 V	-0.13 ± 0.05	0.05 ± 0.06	0.04 ± 0.05	-0.10 ± 0.09	-0.20 ± 0.14	-0.22 ± 0.10	-0.21 ± 0.11	-0.19 ± 0.03	-0.16 ± 0.04	
14446-2215	HD 129715	14:44:35.5	-22:15:11	K2 V	...	-0.16 ± 0.31	-0.11 ± 0.28	0.25 ± 0.33	0.67 ± 0.21	0.22 ± 0.11	0.16 ± 0.09	0.31 ± 0.16	0.28 ± 0.16	
14493+4950	HD 130986 A	14:49:18.1	+49:50:16	F8 V+	-0.01 ± 0.04	0.20 ± 0.10	0.16 ± 0.09	0.03 ± 0.12	0.17 ± 0.09	0.03 ± 0.16	0.05 ± 0.18	-0.05 ± 0.08	0.00 ± 0.10	
14575-2125	HD 131977	14:57:28.0	-21:24:56	K4 V	-0.07 ± 0.11	-0.14 ± 0.13	0.25 ± 0.05	-0.08 ± 0.08	-0.11 ± 0.08	-0.03 ± 0.09	-0.08 ± 0.09	
14595+4528	HD 132830	14:59:32.9	+45:27:51	K0 V	-0.21 ± 0.11	-0.04 ± 0.08	0.00 ± 0.08	-0.11 ± 0.08	0.04 ± 0.07	-0.11 ± 0.09	-0.13 ± 0.10	-0.13 ± 0.05	-0.17 ± 0.06	
15123+3939	HD 135144	15:12:17.8	+39:39:21	K3 V	-0.13 ± 0.06	-0.19 ± 0.09	-0.14 ± 0.09	-0.22 ± 0.07	-0.08 ± 0.08	-0.23 ± 0.05	-0.25 ± 0.05	-0.18 ± 0.13	-0.26 ± 0.05	
15131+1808	BD+18 2985	15:13:06.9	+18:08:09	K0 V	-0.31 ± 0.05	-0.15 ± 0.08	-0.10 ± 0.08	-0.20 ± 0.10	-0.04 ± 0.07	-0.22 ± 0.06	-0.25 ± 0.05	-0.16 ± 0.08	-0.22 ± 0.07	
15164+1648	HD 135792 A	15:16:25.6	+16:47:39	G0 V	-0.28 ± 0.03	-0.01 ± 0.04	0.00 ± 0.04	-0.23 ± 0.07	-0.30 ± 0.15	-0.42 ± 0.13	-0.39 ± 0.14	-0.36 ± 0.05	-0.28 ± 0.06	
15204+0015	HD 136378	15:20:26.1	+00:14:41	K1 V	-0.42 ± 0.32	-0.32 ± 0.07	-0.26 ± 0.07	-0.42 ± 0.04	-0.40 ± 0.10	-0.51 ± 0.07	-0.53 ± 0.07	-0.45 ± 0.04	-0.49 ± 0.04	
15211+2534	HD 136655	15:21:09.3	+25:34:02	K2 V	0.16 ± 0.10	0.09 ± 0.19	0.13 ± 0.17	0.19 ± 0.14	0.38 ± 0.11	0.23 ± 0.13	0.20 ± 0.14	0.24 ± 0.07	0.19 ± 0.08	
15282-0921	HD 137763	15:28:09.6	-09:20:53	G9 V	0.08 ± 0.09	0.06 ± 0.08	0.08 ± 0.07	0.06 ± 0.07	0.19 ± 0.07	0.13 ± 0.05	0.11 ± 0.05	0.11 ± 0.06	0.06 ± 0.07	
	HD 137778	15:28:12.2	-09:21:28	K2 V	-0.11 ± 0.06	0.11 ± 0.14	0.15 ± 0.12	0.05 ± 0.12	0.28 ± 0.08	0.18 ± 0.15	0.15 ± 0.16	0.10 ± 0.06	0.04 ± 0.06	
15289+5727	HD 138367	15:28:51.9	+57:26:43	F7 V	-0.02 ± 0.07	0.06 ± 0.11	0.05 ± 0.10	0.05 ± 0.17	0.19 ± 0.12	-0.13 ± 0.12	-0.11 ± 0.14	-0.08 ± 0.08	-0.05 ± 0.08	
15353+6005	HD 139477	15:35:20.0	+60:05:13	K3 V	...	-0.11 ± 0.24	-0.05 ± 0.23	-0.19 ± 0.17	0.09 ± 0.18	-0.16 ± 0.12	-0.19 ± 0.11	-0.17 ± 0.09	-0.23 ± 0.11	
15431-1303	HD 140269	15:43:08.7	-13:03:23	G1 V	-0.03 ± 0.04	0.19 ± 0.13	0.14 ± 0.12	0.00 ± 0.14	0.01 ± 0.05	-0.22 ± 0.11	-0.19 ± 0.13	-0.18 ± 0.14	-0.21 ± 0.10	
15482+0134	V382 Ser	15:48:09.5	+01:34:18	G8 V	-0.21 ± 0.16	-0.03 ± 0.06	0.01 ± 0.06	-0.14 ± 0.07	-0.06 ± 0.06	-0.07 ± 0.15	-0.09 ± 0.16	-0.18 ± 0.05	-0.23 ± 0.06	
16024+0339	HD 143809	16:02:22.4	+03:39:07	G0 V+	Fast
16048+3910	HD 144579 A	16:04:56.8	+39:09:23	G8 V	-0.51 ± 0.03	-0.15 ± 0.05	-0.09 ± 0.05	-0.49 ± 0.14	-0.52 ± 0.11	-0.89 ± 0.13	-0.90 ± 0.14	-0.59 ± 0.08	-0.59 ± 0.04	
16147+3352	σ CrB B	16:14:40.4	+33:51:27	G1 V	-0.13 ± 0.07	0.07 ± 0.05	0.07 ± 0.04	-0.07 ± 0.10	-0.09 ± 0.09	-0.11 ± 0.05	-0.11 ± 0.05	-0.14 ± 0.04	-0.13 ± 0.05	
16150+6040	HD 146868	16:14:57.1	+60:40:11	G5 V	-0.23 ± 0.08	-0.12 ± 0.05	-0.09 ± 0.04	-0.28 ± 0.07	-0.30 ± 0.08	-0.39 ± 0.07	-0.40 ± 0.08	-0.36 ± 0.04	-0.34 ± 0.03	
16175+7545	η UMi A	16:17:30.3	+75:45:19	F5 V	Fast
16329+0315	HD 149162	16:32:51.6	+03:14:46	K1 V+	-0.08 ± 0.14	-0.08 ± 0.09	-0.04 ± 0.09	0.01 ± 0.13	0.06 ± 0.10	-0.03 ± 0.08	-0.06 ± 0.08	0.01 ± 0.10	-0.04 ± 0.13	
16348-0412	HD 149414 Aa,Ab	16:34:42.4	-04:13:45	G8 V	-0.58 ± 0.15	-0.51 ± 0.13	-0.44 ± 0.13	-1.04 ± 0.19	-0.90 ± 0.13	-1.40 ± 0.16	-1.36 ± 0.14	-1.03 ± 0.15	-0.98 ± 0.18	

Table A1 – continued

WDS	Primary	RA (J2000)	DEC (J2000)	Spectral type	[C/H] (dex)	[O/H] ^{LTE} (dex)	[O/H] ^{NLTE} (dex)	[Sc/H] (dex)	[V/H] (dex)	[Mn/H] ^{LTE} (dex)	[Mn/H] ^{NLTE} (dex)	[Co/H] ^{LTE} (dex)	[Co/H] ^{NLTE} (dex)	Notes ^a
17050-0504	HD 154363 A	17:05:03.4	-05:03:59	K5 V	0.01 ± 0.19	-0.60 ± 0.15	0.17 ± 0.20	-0.69 ± 0.16	-0.77 ± 0.10	-0.37 ± 0.21	-0.38 ± 0.19	
17178+5227	HD 156985	17:17:50.4	+52:26:50	K2 V	-0.14 ± 0.08	-0.29 ± 0.11	-0.24 ± 0.10	-0.16 ± 0.13	0.07 ± 0.10	-0.27 ± 0.12	-0.32 ± 0.11	-0.16 ± 0.08	-0.20 ± 0.08	
17272+4213	HD 158415	17:27:13.9	+42:13:05	G5 V	-0.14 ± 0.06	0.11 ± 0.07	0.11 ± 0.06	0.09 ± 0.10	0.14 ± 0.07	0.08 ± 0.06	0.08 ± 0.06	0.03 ± 0.05	0.01 ± 0.07	
17411+7225	HD 161897	17:41:06.7	+72:25:13	G6 V	-0.09 ± 0.04	-0.04 ± 0.04	-0.02 ± 0.04	-0.01 ± 0.08	0.02 ± 0.05	-0.07 ± 0.05	-0.08 ± 0.05	-0.02 ± 0.09	-0.05 ± 0.08	
17428+1646	BD+16 3263	17:42:50.5	+16:45:54	K0 V	-0.20 ± 0.12	-0.05 ± 0.09	-0.01 ± 0.08	-0.24 ± 0.09	-0.15 ± 0.08	-0.33 ± 0.06	-0.34 ± 0.07	-0.30 ± 0.07	-0.32 ± 0.07	
17465+2743	μ^1 Her A	17:46:27.5	+27:43:14	G5 IV+	0.24 ± 0.05	0.37 ± 0.15	0.32 ± 0.13	0.30 ± 0.08	0.27 ± 0.04	0.26 ± 0.06	0.26 ± 0.07	0.27 ± 0.04	0.25 ± 0.05	
17477+2748	BD+27 2891	17:47:39.2	+27:47:40	G0 V	-0.08 ± 0.23	0.08 ± 0.06	0.08 ± 0.05	0.03 ± 0.14	-0.08 ± 0.05	-0.18 ± 0.10	-0.16 ± 0.11	-0.12 ± 0.08	-0.14 ± 0.06	
18006+6833	BD+68 971	18:00:36.1	+68:33:24	K2 V	-0.20 ± 0.20	-0.03 ± 0.05	0.01 ± 0.05	-0.09 ± 0.16	0.03 ± 0.06	-0.05 ± 0.05	-0.08 ± 0.05	-0.07 ± 0.05	-0.11 ± 0.05	
18006+2934	HD 164595 A	18:00:38.9	+29:34:19	G2 V	-0.10 ± 0.07	0.05 ± 0.06	0.06 ± 0.05	-0.05 ± 0.06	-0.15 ± 0.06	-0.14 ± 0.09	-0.13 ± 0.10	-0.12 ± 0.03	-0.12 ± 0.04	
18090+2409	HD 166301	18:08:58.7	+24:09:30	G0 V	-0.08 ± 0.02	0.01 ± 0.07	0.02 ± 0.06	-0.09 ± 0.09	-0.11 ± 0.09	-0.19 ± 0.03	-0.19 ± 0.04	-0.17 ± 0.07	-0.12 ± 0.04	
18131+4129	HD 167389	18:13:07.2	+41:28:31	F8 V	-0.09 ± 0.06	0.04 ± 0.09	0.03 ± 0.07	0.03 ± 0.12	0.05 ± 0.06	-0.04 ± 0.07	-0.03 ± 0.08	-0.04 ± 0.03	-0.04 ± 0.03	
18161+6839	BD+68 986	18:16:04.0	+68:38:55	G8 V	-0.48 ± 0.24	-0.28 ± 0.05	-0.22 ± 0.05	-0.63 ± 0.10	-0.69 ± 0.10	-0.94 ± 0.11	-0.95 ± 0.12	-0.67 ± 0.12	-0.64 ± 0.10	
18292+1142	HD 170469	18:29:11.0	+11:41:44	G5 V	0.25 ± 0.03	0.39 ± 0.13	0.35 ± 0.11	0.37 ± 0.08	0.26 ± 0.07	0.33 ± 0.07	0.33 ± 0.08	0.31 ± 0.04	0.29 ± 0.05	
18333+2219	HD 171314 A	18:33:17.8	+22:18:51	K4 V	...	-0.33 ± 0.20	-0.27 ± 0.20	0.03 ± 0.22	0.35 ± 0.17	-0.06 ± 0.08	-0.11 ± 0.06	0.04 ± 0.15	0.00 ± 0.14	
18409+3132	BD+31 3330 A	18:40:54.9	+31:31:59	K2.5 V	...	-0.41 ± 0.11	-0.35 ± 0.10	-0.42 ± 0.11	-0.22 ± 0.08	-0.52 ± 0.11	-0.57 ± 0.11	-0.41 ± 0.07	-0.45 ± 0.06	
19321-1116	HD 183870 A	19:32:06.7	-11:16:30	K2 V	...	-0.07 ± 0.09	-0.02 ± 0.09	-0.14 ± 0.09	-0.11 ± 0.09	-0.14 ± 0.14	-0.18 ± 0.15	-0.16 ± 0.06	-0.23 ± 0.07	
19510+1025	σ Aql A	19:51:01.6	+10:24:57	F8 V	0.04 ± 0.06	0.34 ± 0.16	0.25 ± 0.13	0.18 ± 0.09	0.17 ± 0.13	0.08 ± 0.07	0.10 ± 0.07	0.04 ± 0.05	0.05 ± 0.03	
19553+0624	β Aql A	19:55:18.8	+06:24:24	G9.5 IV	-0.29 ± 0.11	-0.08 ± 0.13	-0.07 ± 0.11	-0.13 ± 0.04	-0.09 ± 0.07	-0.25 ± 0.10	-0.25 ± 0.11	-0.12 ± 0.11	-0.17 ± 0.03	
20007+2243	V452 Vul	20:00:43.7	+22:42:39	K0 V	-0.10 ± 0.06	-0.01 ± 0.1	0.04 ± 0.10	-0.12 ± 0.14	0.07 ± 0.08	-0.05 ± 0.20	-0.05 ± 0.21	-0.12 ± 0.10	-0.15 ± 0.04	
20036+2954	HD 190360 A	20:03:37.4	+29:53:48	G7 V	0.20 ± 0.05	0.34 ± 0.10	0.33 ± 0.09	0.26 ± 0.09	0.27 ± 0.06	0.25 ± 0.13	0.25 ± 0.13	0.25 ± 0.05	0.23 ± 0.07	
20111+1611	HD 191785	20:11:06.1	+16:11:17	K0 V	-0.07 ± 0.05	0.14 ± 0.07	0.19 ± 0.06	-0.07 ± 0.09	0.06 ± 0.07	-0.24 ± 0.04	-0.26 ± 0.05	-0.05 ± 0.05	-0.09 ± 0.05	
20124-1237	ξ Cap	20:12:25.9	-12:37:03	F7 V	-0.21 ± 0.05	0.07 ± 0.10	0.04 ± 0.09	-0.09 ± 0.11	...	-0.32 ± 0.18	-0.30 ± 0.18	-0.20 ± 0.10	-0.13 ± 0.06	
20169+5017	HD 193216 Aa,Ab	20:16:54.5	+50:16:43	G5 V	-0.01 ± 0.06	0.26 ± 0.06	0.29 ± 0.05	0.04 ± 0.14	0.04 ± 0.06	-0.03 ± 0.04	-0.04 ± 0.04	0.03 ± 0.05	0.00 ± 0.06	
20408+1956	HD 197076 A	20:40:45.1	+19:56:08	G1 V	-0.18 ± 0.02	0.04 ± 0.05	0.05 ± 0.04	-0.02 ± 0.12	-0.19 ± 0.09	-0.22 ± 0.06	-0.22 ± 0.07	-0.17 ± 0.04	-0.15 ± 0.05	
20462+3358	ϵ Cyg A	20:46:12.7	+33:58:13	K0 III+	-0.35 ± 0.06	0.07 ± 0.20	0.04 ± 0.17	-0.10 ± 0.07	-0.03 ± 0.07	-0.19 ± 0.06	-0.18 ± 0.07	-0.09 ± 0.09	-0.10 ± 0.07	
20473+1052	BD+10 4379	20:47:16.8	+10:51:37	K2 V	-0.429 ± 0.11	-0.52 ± 0.11	0.10 ± 0.05	-0.66 ± 0.11	-0.69 ± 0.12	-0.42 ± 0.15	-0.45 ± 0.10	
20599+4016	HD 200077	20:59:55.3	+40:15:32	F8 V+	-0.26 ± 0.09	-0.20 ± 0.08	-0.24 ± 0.07	-0.10 ± 0.11	-0.09 ± 0.10	-0.20 ± 0.09	-0.16 ± 0.09	-0.29 ± 0.09	-0.26 ± 0.04	SB2
21324-2058	HD 204941	21:32:23.5	-20:57:27	K2 V	-0.37 ± 0.05	-0.09 ± 0.07	-0.04 ± 0.07	-0.16 ± 0.06	-0.10 ± 0.08	-0.23 ± 0.06	-0.26 ± 0.06	-0.20 ± 0.09	-0.23 ± 0.08	
21519+4221	HD 207966 A	21:51:52.9	+42:20:38	G8 V	-0.11 ± 0.06	-0.02 ± 0.08	0.01 ± 0.07	-0.10 ± 0.08	0.01 ± 0.06	-0.10 ± 0.05	-0.12 ± 0.05	-0.08 ± 0.05	-0.10 ± 0.05	
21546-0318	HD 208177	21:54:35.9	-03:18:05	F6 V	Fast
21575+2856	BD+28 4248	21:57:30.8	+28:56:13	G5 V	0.03 ± 0.04	0.23 ± 0.08	0.21 ± 0.07	0.12 ± 0.09	0.12 ± 0.11	0.10 ± 0.07	0.09 ± 0.08	0.08 ± 0.06	0.08 ± 0.06	
22066+4323	BD+42 4301	22:06:36.6	+43:22:33	G3 V	0.20 ± 0.04	0.17 ± 0.08	0.16 ± 0.08	0.28 ± 0.05	0.26 ± 0.04	0.27 ± 0.09	0.26 ± 0.10	0.25 ± 0.05	0.23 ± 0.06	
22090-1754	HD 210190	22:08:58.7	-17:53:40	K0 V	-0.35 ± 0.47	-0.19 ± 0.11	-0.14 ± 0.08	-0.34 ± 0.13	-0.35 ± 0.07	-0.46 ± 0.06	-0.48 ± 0.06	-0.41 ± 0.04	-0.43 ± 0.04	
22159+5440	V447 Lac	22:15:54.1	+54:40:22	K1 V	-0.17 ± 0.17	0.01 ± 0.05	0.05 ± 0.05	-0.12 ± 0.07	0.01 ± 0.07	-0.05 ± 0.11	-0.06 ± 0.12	-0.14 ± 0.05	-0.18 ± 0.06	
22311+4509	HD 213519 A	22:31:05.7	+45:08:42	G5	0.01 ± 0.06	0.09 ± 0.09	0.09 ± 0.08	-0.03 ± 0.09	-0.09 ± 0.07	-0.05 ± 0.05	-0.05 ± 0.05	-0.03 ± 0.06	-0.02 ± 0.06	
22467+1210	ξ Peg A	22:46:41.6	+12:10:22	F6 V	-0.19 ± 0.04	0.07 ± 0.10	0.02 ± 0.09	-0.14 ± 0.08	...	-0.32 ± 0.12	-0.26 ± 0.12	-0.20 ± 0.16	-0.07 ± 0.16	
22524+0950	σ Peg A	22:52:24.1	+09:50:08	F6 V	-0.12 ± 0.05	0.22 ± 0.12	0.14 ± 0.11	-0.10 ± 0.06	-0.17 ± 0.36	-0.23 ± 0.16	-0.16 ± 0.17	-0.14 ± 0.14	-0.05 ± 0.11	
22589+6902	BD+68 1345 A	22:58:53.8	+69:01:50	K0 V	-0.12 ± 0.12	-0.04 ± 0.09	0.00 ± 0.07	-0.08 ± 0.05	-0.04 ± 0.07	-0.12 ± 0.05	-0.13 ± 0.05	-0.08 ± 0.05	-0.13 ± 0.06	
23026+2948	BD+29 4841 Aa,Ab	23:02:34.6	+29:48:18	K0 V	SB2
23104+4901	HD 218790	23:10:21.3	+49:01:06	G0 V	0.22 ± 0.02	0.38 ± 0.12	0.32 ± 0.10	0.33 ± 0.11	0.26 ± 0.06	0.26 ± 0.07	0.26 ± 0.08	0.28 ± 0.03	0.29 ± 0.03	
23194+7900	V368 Cep	23:19:26.6	+79:00:13	G9 V	Fast
23235+4548	HD 220445	23:23:28.8	+45:47:36	K0 V	...	-0.03 ± 0.14	0.02 ± 0.13	0.04 ± 0.11	0.24 ± 0.12	0.05 ± 0.06	0.02 ± 0.06	0.03 ± 0.07	-0.02 ± 0.08	
23266+4520	HD 220821	23:26:40.6	+45:20:17	G0 V+	-0.16 ± 0.11	-0.02 ± 0.06	-0.02 ± 0.05	-0.17 ± 0.08	-0.08 ± 0.07	-0.19 ± 0.15	-0.17 ± 0.16	-0.24 ± 0.05	-0.21 ± 0.06	
23355+3101	HD 221830 A	23:35:28.9	+31:01:02	F9 V	-0.24 ± 0.04	0.10 ± 0.05	0.12 ± 0.04	-0.15 ± 0.10	-0.24 ± 0.10	-0.58 ± 0.15	-0.56 ± 0.16	-0.30 ± 0.06	-0.25 ± 0.07	
23419-0559	HD 222582 A	23:41:51.5	-05:59:09	G5 V	-0.01 ± 0.06	0.12 ± 0.08	0.12 ± 0.07	0.03 ± 0.07	-0.03 ± 0.07	-0.08 ± 0.05	-0.08 ± 0.06	-0.01 ± 0.04	0.00 ± 0.03	
23536+1207	MCC 870	23:53:35.5	+12:06:22	K4 V	-0.52 ± 0.38	0.42 ± 0.32	-0.47 ± 0.27	-0.55 ± 0.26	-0.37 ± 0.22	-0.36 ± 0.20	
23556+0042	HD 224157	23:55:36.0	+00:41:45	K0 V	-0.05 ± 0.17	0.08 ± 0.15	0.11 ± 0.12	-0.02 ± 0.09	0.13 ± 0.06	0.07 ± 0.06	0.05 ± 0.06	0.03 ± 0.05	-0.01 ± 0.06	
23581+2420	HD 224459 Aa,Ab	23:58:03.9	+24:20:28	G2	SB2
	BD+23 4830 B	23:58:03.4	+24:20:33	K0 V	-0.09 ± 0.05	-0.02 ± 0.08	0.02 ± 0.07	-0.14 ± 0.09	-0.05 ± 0.06	-0.11 ± 0.03	-0.12 ± 0.04	-0.14 ± 0.06	-0.17 ± 0.06	

^a SB2: Double-line spectroscopic binary; Hot: Spectral type ≤ F6 V; Cool: Spectral type ≥ K4 V; Fast: $v \sin i \geq 10 \text{ km s}^{-1}$

Table A2. HFS components for the Sc lines.

Sc I 5520.519		Sc I 5671.860		Sc II 5526.789		Sc II 5657.886		Sc II 5667.135		Sc II 5684.190		Sc II 6245.621		Sc II 6320.832	
λ (Å)	$\log(gf)$	λ (Å)	$\log(gf)$	λ (Å)	$\log(gf)$	λ (Å)	$\log(gf)$	λ (Å)	$\log(gf)$	λ (Å)	$\log(gf)$	λ (Å)	$\log(gf)$	λ (Å)	$\log(gf)$
5520.482	-0.339	5671.773	-0.926	5526.770	-2.805	5657.886	-1.166	5667.135	-1.804	5684.190	-1.553	6245.621	-1.624	6320.832	-2.410
5520.494	-0.339	5671.778	-0.808	5526.775	-2.402	5657.887	-1.736	5667.141	-2.000	5684.192	-2.042	6245.629	-2.364	6320.839	-2.606
5520.508	-0.339	5671.779	-1.378	5526.779	-1.592	5657.892	-1.736	5667.148	-2.000	5684.193	-2.741	6245.631	-1.795	6320.850	-2.606
5520.519	-0.339	5671.785	-0.690	5526.779	-2.190	5657.894	-1.564	5667.153	-3.185	5684.204	-1.846	6245.636	-3.364	6320.857	-3.791
		5671.787	-1.167	5526.782	-1.387	5657.895	-1.578	5667.157	-2.004	5684.206	-1.926	6245.638	-2.181	6320.862	-2.610
		5671.788	-2.378	5526.783	-2.080	5657.899	-1.578	5667.162	-2.004	5684.207	-2.301	6245.640	-2.002	6320.871	-2.610
		5671.795	-0.578	5526.785	-1.321	5657.900	-2.260	5667.166	-2.259	5684.215	-2.301	6245.644	-2.946	6320.876	-2.865
		5671.797	-1.071	5526.786	-2.059	5657.901	-1.589			5684.216	-2.046	6245.645	-2.148		
		5671.799	-2.171	5526.788	-1.325	5657.904	-1.589			5684.217	-2.030	6245.647	-2.273		
		5671.807	-0.474	5526.789	-0.663	5657.905	-3.686					6245.650	-2.712		
		5671.810	-1.035	5526.789	-2.168	5657.906	-1.762					6245.651	-2.207		
		5671.813	-2.143	5526.790	-1.386	5657.908	-1.762					6245.652	-2.691		
		5671.822	-0.378	5526.791	-0.784	5657.909	-1.938					6245.654	-2.566		
		5671.826	-1.051	5526.791	-1.508							6245.655	-2.390		
		5671.829	-2.223	5526.792	-1.691							6245.657	-2.469		
		5671.840	-0.288	5526.793	-0.920										
		5671.844	-1.133	5526.794	-1.076										
		5671.847	-2.415	5526.794	-1.837										
		5671.860	-0.204	5526.795	-1.261										
		5671.864	-1.351	5526.795	-1.495										
		5671.868	-2.804												

Table A3. HFS components for the V lines.

V I 5670.831		V I 5737.027		V I 6081.461		V I 6224.520		V I 6251.802		V I 6274.659		V I 6285.162			
λ (Å)	$\log(gf)$	λ (Å)	$\log(gf)$	λ (Å)	$\log(gf)$	λ (Å)	$\log(gf)$	λ (Å)	$\log(gf)$	λ (Å)	$\log(gf)$	λ (Å)	$\log(gf)$		
5670.811	-1.103	5737.027	-1.386	6081.418	-1.814	6224.486	-3.594	6251.767	-2.954	6274.611	-2.962	6285.108	-3.598		
5670.819	-2.111	5737.037	-2.085	6081.418	-1.638	6224.495	-3.390	6251.784	-2.750	6274.632	-2.485	6285.128	-3.170		
5670.826	-3.412	5737.041	-2.085	6081.428	-1.638	6224.504	-3.325	6251.799	-2.685	6274.644	-2.506	6285.133	-2.733		
5670.831	-1.208	5737.051	-1.678	6081.429	-2.610	6224.513	-3.332	6251.802	-2.051	6274.659	-2.164	6285.144	-2.920		
5670.838	-1.900	5737.059	-1.904	6081.429	-1.513	6224.520	-2.691	6251.813	-2.692	6274.660	-2.485	6285.147	-2.572		
5670.844	-3.014	5737.063	-1.904	6081.443	-1.513	6224.521	-3.398	6251.814	-2.238	6274.682	-2.631	6285.158	-2.744		
5670.848	-1.324	5737.070	-2.084	6081.443	-1.832	6224.525	-2.878	6251.824	-2.457			6285.159	-2.580		
5670.855	-1.827	5737.077	-1.873	6081.444	-1.627	6224.528	-3.536	6251.825	-2.758			6285.162	-2.107		
5670.860	-2.810	5737.080	-1.873	6081.461	-1.627	6224.529	-3.097	6251.833	-2.720			6285.168	-2.744		
5670.863	-1.453	5737.086	-2.801	6081.461	-1.216	6224.533	-3.360	6251.835	-2.896			6285.172	-2.323		
5670.868	-1.821	5737.091	-1.937			6224.534	-3.816	6251.840	-3.051			6285.179	-2.606		
5670.872	-2.713	5737.093	-1.937			6224.535	-3.691	6251.844	-3.176			6285.182	-3.045		
5670.875	-1.599	5737.098	-4.044			6224.537	-4.138	6251.845	-3.498						
5670.879	-1.868	5737.101	-2.136			6224.539	-4.837	6251.849	-4.197						
5670.882	-2.713	5737.103	-2.136			6224.544	-3.816	6251.849	-2.954						
5670.884	-1.769	5737.106	-2.391			6224.549	-3.536	6251.854	-2.750						
5670.887	-1.973					6224.552	-3.398	6251.855	-3.176						
5670.890	-2.868					6224.555	-3.332	6251.858	-2.685						
5670.891	-1.973					6224.557	-3.325	6251.858	-2.896						
5670.893	-2.169					6224.559	-3.390	6251.860	-2.692						
5670.895	-2.236					6224.560	-3.594	6251.860	-2.758						

Table A4. HFS components for the Mn lines.

Mn I 4502.204		Mn I 4671.647		Mn I 4739.072		Mn I 5377.626		Mn I 5399.500		Mn I 5413.697	
λ (Å)	$\log(gf)$	λ (Å)	$\log(gf)$	λ (Å)	$\log(gf)$	λ (Å)	$\log(gf)$	λ (Å)	$\log(gf)$	λ (Å)	$\log(gf)$
4502.204	-0.912	4671.647	-2.242	4739.070	-1.635	5377.564	-1.576	5399.423	-1.403	5413.593	-1.981
4502.207	-1.830	4671.654	-3.160	4739.072	-1.158	5377.576	-1.166	5399.429	-1.271	5413.628	-1.550
4502.208	-3.047	4671.660	-4.377	4739.090	-1.533	5377.576	-1.400	5399.439	-1.771	5413.638	-1.437
4502.211	-1.052	4671.664	-2.382	4739.091	-1.707	5377.582	-1.722	5399.441	-1.373	5413.658	-1.437
4502.213	-1.654	4671.670	-2.984	4739.093	-1.635	5377.594	-1.245	5399.453	-2.980	5413.697	-1.073
4502.213	-2.695	4671.675	-4.025	4739.105	-1.665	5377.596	-0.893	5399.468	-1.403	5413.702	-1.534
4502.216	-1.210	4671.678	-2.540	4739.106	-3.242	5377.606	-1.768	5399.473	-1.445		
4502.217	-1.628	4671.683	-2.958	4739.107	-1.533	5377.620	-1.224	5399.497	-1.271		
4502.217	-2.570	4671.687	-3.900	4739.115	-2.033	5377.626	-0.681	5399.500	-0.896		
4502.220	-1.394	4671.689	-2.724	4739.116	-1.665	5377.637	-1.944	5399.532	-1.373		
4502.220	-1.695	4671.693	-3.025			5377.655	-1.370				
4502.220	-2.649	4671.695	-3.979			5377.678	-2.324				
4502.222	-1.616	4671.697	-2.946								
4502.222	-1.871	4671.699	-3.201								
4502.223	-1.901	4671.701	-3.231								

Table A5. HFS components for the Co lines.

Co I 4594.669		Co I 4792.854		Co I 4813.471		Co I 5301.017		Co I 5342.706		Co I 5352.020		Co I 5359.188		Co I 5647.207		Co I 6814.958	
λ (Å)	$\log(gf)$	λ (Å)	$\log(gf)$	λ (Å)	$\log(gf)$	λ (Å)	$\log(gf)$	λ (Å)	$\log(gf)$	λ (Å)	$\log(gf)$	λ (Å)	$\log(gf)$	λ (Å)	$\log(gf)$	λ (Å)	$\log(gf)$
4594.582	-1.848	4792.799	-2.583	4813.398	-2.862	5301.008	-3.345	5342.693	-0.459	5351.893	-3.244	5359.188	-0.429	5647.207	-2.127	6814.889	-2.917
4594.583	-1.568	4792.814	-2.173	4813.416	-2.464	5301.017	-2.646	5342.693	-0.542	5351.925	-2.855	5359.191	-0.534	5647.220	-2.343	6814.915	-2.803
4594.587	-1.430	4792.824	-1.469	4813.432	-1.561	5301.026	-3.164	5342.693	-0.373	5351.953	-1.791	5359.194	-0.650	5647.232	-2.626	6814.924	-2.506
4594.588	-2.869	4792.827	-1.951	4813.432	-2.260	5301.034	-2.938	5342.694	-0.289	5351.976	-1.573	5359.197	-0.779	5647.238	-2.753	6814.936	-2.928
4594.590	-1.848	4792.834	-1.273	4813.445	-1.350	5301.040	-3.133	5342.696	-0.208	5351.978	-2.583	5359.200	-0.925	5647.243	-3.065	6814.943	-3.122
4594.593	-1.364	4792.838	-1.826	4813.447	-2.163	5301.043	-3.345	5342.699	-0.130	5351.997	-1.491	5359.203	-1.095	5647.246	-2.592	6814.958	-2.190
4594.594	-2.170	4792.843	-1.219	4813.456	-1.277	5301.047	-3.344	5342.701	-1.267	5352.000	-2.611	5359.207	-1.299	5647.253	-2.600	6814.969	-3.104
4594.598	-1.568	4792.848	-1.775	4813.459	-2.163	5301.052	-3.197	5342.702	-0.056	5352.014	-1.475	5359.210	-1.562	5647.259	-2.764	6814.978	-2.917
4594.603	-1.723	4792.850	-1.241	4813.466	-1.271	5301.056	-3.164	5342.704	-1.049	5352.019	-2.818	5359.214	-1.495	5647.264	-3.618	6814.987	-2.803
4594.603	-1.357	4792.854	-0.629	4813.470	-2.318	5301.058	-4.061	5342.706	+0.014	5352.020	-0.644	5359.214	-1.299	5647.267	-3.190	6814.991	-2.928
4594.610	-1.430	4792.855	-1.805	4813.471	-0.553	5301.062	-3.396	5342.707	-0.955	5352.029	-1.511	5359.215	-1.194	5647.269	-2.940		
4594.615	-1.392	4792.856	-1.332	4813.473	-1.318	5301.065	-3.133	5342.711	-0.923	5352.036	-0.728	5359.215	-1.147	5647.269	-2.764		
4594.616	-1.422	4792.860	-1.520	4813.478	-0.658	5301.065	-5.304	5342.713	-2.480	5352.041	-1.607	5359.216	-1.153				
4594.624	-1.364	4792.860	-0.770	4813.479	-1.423	5301.070	-3.651	5342.716	-0.943	5352.048	-0.818	5359.216	-1.226				
4594.630	-1.129	4792.864	-0.934	4813.483	-0.934	5301.071	-3.197	5342.718	-2.246	5352.050	-1.818	5359.217	-1.437				
4594.631	-1.626	4792.867	-1.132	4813.485	-0.774	5301.074	-3.396	5342.722	-1.030	5352.059	-0.914	5359.221	-2.194				
4594.641	-1.357	4792.868	-1.775	4813.489	-0.903			5342.725	-2.200	5352.066	-1.018	5359.225	-2.039				
4594.648	-0.910	4792.868	-1.387	4813.490	-1.686			5342.728	-1.253	5352.070	-1.130	5359.229	-2.039				
4594.661	-1.422			4813.492	-1.049			5342.731	-2.267	5352.070	-1.366	5359.234	-2.136				
4594.669	-0.723			4813.493	-1.423			5342.739	-2.450	5352.072	-1.248	5359.238	-2.340				
4594.685	-1.626			4813.493	-1.219			5342.747	-2.832			5359.242	-2.738				

This paper has been typeset from a \TeX/L\AA\TeX file prepared by the author.